
Modular design of ionotropic glutamate receptors: Coupling of a viral K⁺-channel with a glutamate-binding domain

The relation between rudimental potassium channel and high developed glutamate receptors

Vom Fachbereich
Biologie



TECHNISCHE
UNIVERSITÄT
DARMSTADT

der Technischen Universität Darmstadt
zur Erlangung des akademischen Grades eines
Doctor rerum naturalium
genehmigte Dissertation

von
M. Sc. Michael Schönrock
geboren am 23.12.1988
in Heidelberg

Erstgutachter: Prof. Dr. Bodo Laube
Zweitgutachter: Prof. Dr. Gerhard Thiel

Tag der Einreichung: 21.01.2019
Tag der mündlichen Prüfung: 13.03.2019

Darmstadt 2019

D17

Schönrock, Michael: "Modular design of ionotropic glutamate receptors: Coupling of a viral K⁺-channel with a glutamate-binding domain"
Darmstadt, Technische Universität Darmstadt
Jahr der Veröffentlichung der Dissertation auf TUprints: 2019
URN: nbn:de:tuda-tuprints-85562
Tag der mündlichen Prüfung:13.03.2019

Veröffentlicht unter CC BY-NC-ND 4.0 International
<https://creativecommons.org/licenses/>

Ehrenwörtliche Erklärung

Ich erkläre hiermit ehrenwörtlich, dass ich die vorliegende Arbeit entsprechend den Regeln guter wissenschaftlicher Praxis selbstständig und ohne unzulässige Hilfe Dritter angefertigt habe.

Sämtliche aus fremden Quellen direkt oder indirekt übernommenen Gedanken sowie sämtliche von Anderen direkt oder indirekt übernommenen Daten, Techniken und Materialien sind als solche kenntlich gemacht. Die Arbeit wurde bisher bei keiner anderen Hochschule zu Prüfungszwecken eingereicht.

Darmstadt, den 21.01.2019

.....



I. Table of Contents

I. Table of Contents	1
II. ... Summary	3
III. .. Zusammenfassung	4
1. Introduction	5
1.1. Potassium channels	5
1.2. Classes of potassium channels	6
1.3. General structure of potassium channel and the selectivity filter	7
1.3.1. Modularity	8
1.4. Chlorella virus potassium channel (Kcv)	9
1.5. Prokaryotic substrate-binding proteins	9
1.6. Glutamate receptor	10
1.7. Classes of GluRs	11
1.8. Activating mechanisms in AMPA receptor	12
1.9. Role of NTD and TMDc in GluRs	13
1.10. The relation between IGluR and potassium channel	13
1.11. Aim of this work	15
2. Material and Methods	16
2.1. Cloning and mutagenesis	16
2.2. Cultivation and transfection of HEK293 cells	17
2.3. Immunofluorescence staining	18
2.4. CLSM	18
2.5. Patch clamp recordings	19
2.6. Oocyte expression and TEVC	19
2.7. Protein production and Bilayer measurements	20
2.8. Prediction of the protein-orientation within the membrane	21
2.9. Structure model	21
2.10. Analysis	21
3. Project I - Orientation of KCV _{ATCV-1} channel in the cell membrane of HEK293 cells	22
3.1. Introduction	22
3.2. Results	24

3.2.1.	Influence of signal peptides to the electrophysiological response of Kcv _{ATCV-1}	24
3.2.2.	Determination of the channel orientation of Kcv _{ATCV-1} by immunostaining	30
3.3.	Discussion	34
4.	Project II - Fusion of Kcv _{ATCV-1} with AMPA receptor - A ligand gated potassium channel chimera	37
4.1.	Introduction	37
4.2.	Results	40
4.2.1.	Construction of glutamate-gated GluA1/Kcv _{ATCV-1} chimeras	40
4.2.2.	Increase of glutamate efficacy	43
4.2.3.	Pharmacological characterization of the GluATCV*	45
4.3.	Discussion	48
5.	Project III - Reduction of the chimera on the core parts of a receptor	51
5.1.	Introduction	51
5.2.	Results	52
5.2.1.	Design of a minimal glutamate-gated potassium channel	52
5.3.	Discussion	55
6.	Conclusion	57
7.	Supplement	60
8.	Illustration directory	63
9.	List of abbreviations	64
10. ...	References	66
11. ..	Curriculum Vitae	74
12. ...	Acknowledgement	75

II. Summary

Ionotropic glutamate receptors form the basic structures for rapid excitatory signal transmission in the central nervous system. After the binding of a ligand and the resulting pore opening, they allow an ion flow across the membrane. From an evolutionary point of view, these are highly developed and highly complex structures composed of different domains. There is a ligand binding domain necessary for ligand recognition coupled to the pore which is responsible for the real ion conduction. Extracellular additionally the n-terminal domain and intracellular the c-terminal is located both involved in modulational tasks where the n-terminus should also be responsible for the assembly.

Due to the structural similarity and overlaps in the sequence, it has been assumed for years that these highly engineered receptors originally evolved through a fusion of substrate binding proteins and upturned potassium channels. However, attempting to rebuild a glutamate receptor to a potassium selective one or even to install a potassium channel failed. GluR0, a bacterial glutamate receptor, shows an increased potassium selectivity what is a further indication for this theory but could not be merged with mammalian receptor so far.

In the first chapter I can show that it is possible to insert a rudimentary potassium channel (KcV_{ATCV-1}) in an inverted orientation into the cell membrane. This property fits perfect to the idea to exchange the pore of a glutamate receptor to make it potassium selective. In the second chapter I designed a chimera out of a KcV_{ATCV-1} and a highly developed glutamate receptor (GluA1). Using this chimera, I demonstrated that it is possible to gate a potassium channel by the gating machinery of a glutamate receptor. In this chimeric receptor the most important pharmacological parameters of the GluA1 are obtained even though the selectivity of the KcV_{ATCV-1} is transferred. The studied main characteristics of the potassium channel, the barium block and also the selectivity are still present as well as the effects of certain mutations on channel behavior. In turn, the chimera still reacts to the same agonists and antagonists as the origin receptor. Interestingly, not even the apparent affinity for the tested agonists and antagonists was affected in the chimeric receptor. In the third chapter, a connection to the bacterial GluR0 could be opened. Mammalian wild-type receptors, unlike GluR0, possess an essential extra transmembrane domain. Removing of this extra transmembrane domain in mammalian receptors makes them unfunctional. Interestingly this third TM can be removed in the chimera. A function, albeit with a reduced affinity for glutamate, is still present.

III. Zusammenfassung

Ionotrope Glutamatrezeptoren bilden die Grundstrukturen für eine schnelle erregende Signalübertragung im zentralen Nervensystem. Sie erlauben nach der Bindung eines Liganden und der daraus resultierenden Porenöffnung einen Ionenfluss über die Membran. Evolutiv gesehen handelt es sich hierbei um hochentwickelte und hoch komplexe Strukturen, die aus unterschiedlichen Domänen zusammengesetzt sind. Es gibt eine für die Ligandenerkennung notwendige Ligandenbindungsdomäne, die an eine Pore gekoppelt ist, welche die eigentliche Ionenleitung verantwortet. Zusätzlich hierzu befinden sich extrazellulär die n-terminalen Domäne und intrazellulär die c-terminale Domäne. Beide sind an modulatorischen Aufgaben beteiligt, wobei die n-terminale Domäne auch für die Assemblierung verantwortlich sein soll. Aufgrund der strukturellen Ähnlichkeit von Glutamatrezeptoren mit Substratbindeproteinen und Kaliumkanälen und einer zusätzlichen Überschneidung in ihrer Sequenz wird seit Jahren davon ausgegangen, dass sich diese hoch entwickelten Rezeptoren ursprünglich durch eine Fusion aus beiden entwickelt haben. Der Versuch, einen Glutamatrezeptor zu einem kaliumselektiven Rezeptor umzubauen oder sogar einen Kaliumkanal zu integrieren, scheiterte bisher jedoch. GluR0, ein bakterieller Glutamatrezeptor, zeigt eine erhöhte Kaliumselektivität. Trotz dieses weiteren Hinweises für diese Theorie, konnte weiterhin keine Fusion eines Kaliumkanals mit einem Säugetierrezeptor gezeigt werden. Im ersten Kapitel kann ich zeigen, dass es möglich ist, einen rudimentären Kaliumkanal (KcV_{ATCV-1}) in umgekehrter Ausrichtung in die Zellmembran einzubringen. Diese Eigenschaft passt perfekt zu der Idee, die Pore eines Glutamatrezeptors auszutauschen, um diesen dadurch kaliumselektiv zu machen. Im zweiten Kapitel entwerfe ich eine Chimäre aus einem einfachen KcV_{ATCV-1} und einem hoch entwickelten Glutamatrezeptor (GluA1). Mit dieser Chimäre kann ich zeigen, dass es möglich ist, einen Kaliumkanal durch die Gating-Maschinerie eines Glutamatrezeptors zu steuern. In diesem chimären Rezeptor bleiben die wichtigsten pharmakologischen Parameter des GluA1 erhalten, obwohl die Selektivität des KcV_{ATCV-1} übertragen wird. Die untersuchten Hauptmerkmale des Kaliumkanals, der Bariumblock und auch die Selektivität, sind noch vorhanden ebenso wie die Auswirkungen bestimmter Mutationen auf das Kanalverhalten. Die Chimäre wiederum reagiert immer noch auf die gleichen Agonisten und Antagonisten wie der ursprüngliche Rezeptor. Interessanterweise ist auch die apparente Affinität zu den getesteten Agonisten und Antagonisten im chimären Rezeptor nicht beeinträchtigt. Im dritten Kapitel kann eine Verbindung zum bakteriellen GluR0 hergestellt werden. Säugetier-Rezeptoren besitzen im Gegensatz zum GluR0 eine zusätzliche Transmembrandomäne deren Entfernung diese funktionsunfähig macht. Interessanterweise kann dieses dritte TM in der Chimäre entfernt werden. Eine Funktion, wenn auch mit verminderter Affinität zu Glutamat, ist noch vorhanden.

1. Introduction

A fundamental characteristic of living cells is to enclose their inside by a membrane out of phospholipids and also to separate specialized compartments by membranes. This separation allows for example a specification of compartments for individual tasks like the protein translation of the endoplasmic reticulum or the energy generation of mitochondria. Hence, biological membranes are semi permeable which means that some agents like water can pass the membrane without or with a low resistance, but for other like loaded ions it is an insurmountable barrier.

To transport non-permeable agents over the membrane, energy is required. The necessary energy to transport an ion over a membrane would be around 50 kcal/mol (Parsegian 1969), statistically 1 ion in 10^{16} years would pass the membrane spontaneously (Chatelain et al. 2005). This energetically barrier is resolved by ion channels, integral membrane proteins, which form a pore throughout the membrane. Ion channels allows ions to pass the membrane in the direction of a concentration or electrochemical gradient (Lüttge et al. 2010) as they reduce the necessary energy for passing through to 2-3 kcal/mol (Berneche & Roux 2001). In most cases these ion channels are selective just for a particular group/size of ions or just one sort of ion for example potassium. The charge segregation inside and outside of the cell and their selective permeability is crucial for fundamental cellular processes like energy transfer or cell communication.

1.1. Potassium channels

Potassium channels are a widespread ion channel family which are found in eukaryote, bacteria and archaea and even in viruses. As the name indicates they conduct potassium with a high selectivity over other ions for example sodium. Potassium channels play an essential role in the building of the membrane potential. Beside this, potassium channels are involved in even more essential tasks, like cell-cell communication, energy household or generally protein-expression (Hille 2001). Typically, potassium channels are responsible in keeping and stabilizing the membrane potential and was identified for the first-time in the year 1952 by Hodgkin and Huxley (Hodgkin & Huxley 1952) who were working on the membrane potential of squid giant axons. Since the discovery of the first potassium channel wide variety of different potassium channels could be identified, specialized for a lot of different physiological properties. The next big step in potassium channel research was the discovery of the first crystal structure with the bacterial potassium channel KcsA out of *Streptomyces lividans* from MacKinnon and colleagues

(Doyle et al. 1998). This first structural insight allows to visualize special components, for example the working mechanism of the filter domain.

1.2. Classes of potassium channels

There are different species of potassium channel which can be separated in four topological classes. These classes are divided by the number of transmembrane domains which could variate between two to eight transmembrane domains (TMD). The first and smallest class consists of only two TMD per monomer and partially with intracellular domains. Well-known representatives are the bacterial KcsA (Doyle et al. 1998) or the mammalian inward rectifier

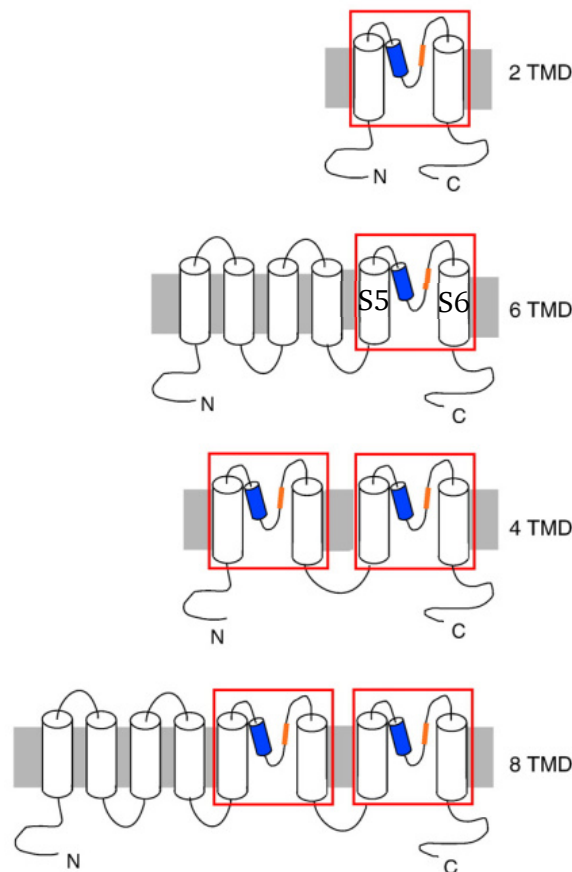


Figure 1 Topology of main potassium channel classes. Each subunit owns at least one pore domain with potential more TM or intercellular domains. Four subunits build together a functional channel. The pore forming region is marked with a red box. The 6 TMD structure represents the group of voltage gated potassium channel. A subunit can also contain two pore forming regions. In cases of two pore forming domains only two subunits are necessary to form a functional channel. (Thiel et al. 2011)

Kir (Hibino et al. 2010). Four subunits of these two TMD monomers build a functional channel. This class also includes the smallest potassium channel like Kcv_{ATCV-1} used in this work. The second class also owns this pore module out of 2 TMD (called S5 S6) and additionally 4 further

TMD. This class is typically voltage sensitive and the TM4 directly before the pore module functions as a voltage sensor by slightly changing its position in the membrane triggered by positive loaded amino acids. An example for this voltage gated potassium channel class are the shaker channels.

The third and fourth group just show two pore domains per subunit and are really similar to the first two groups. This tandem called channels need just two subunits to form a canonical pore (Thiel et al. 2011; Wood et al. 1995).

1.3. General structure of potassium channel and the selectivity filter

Potassium channels are tetramers, built out of four subunits. Each subunit consists at least out of two TMDs and a pore loop. All four subunits together form a water filled pore through the cell membrane. In case of voltage gated potassium channels, four additional domains wrap the pore and the TM4 forms the voltage sensing domain. The pore region is built by the TM1 and TM2, in voltage gated channel S5 and S6, which are connected with a small helix and a linker. A conserved sequence - TxxTxG Y/F G - called signature or filter sequence is part of this linker. All potassium channel known to date, harbor this linker sequence and is assumed as a typical characteristic for potassium selectivity (Heginbotham et al. 1994). The five amino acids motive

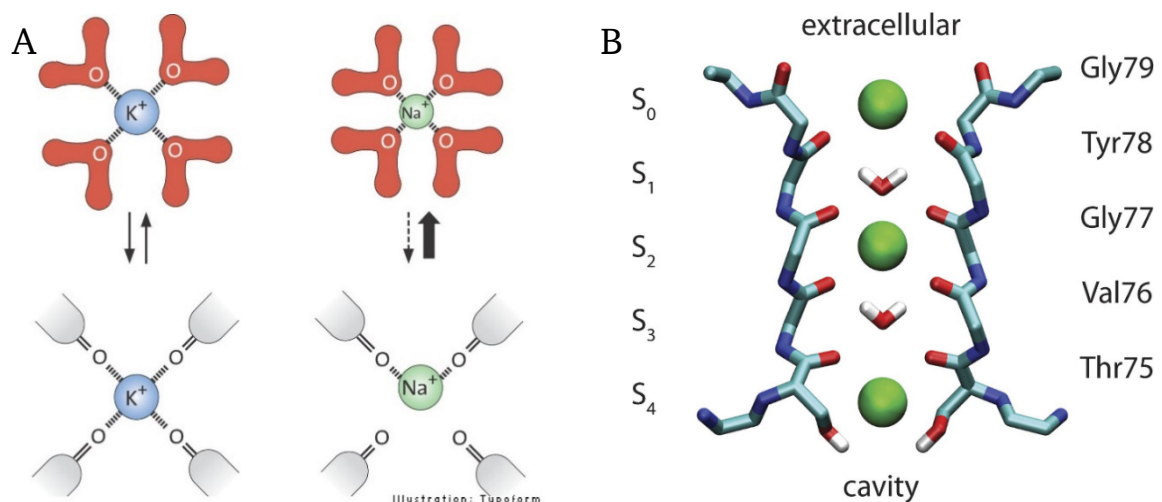


Figure 2 Selectivity filter in potassium channels. A) the potassium filter is ensured by four oxygens which mimic the hydrate shell of a potassium ion. The distance of potassium ions to their hydrate shell fits perfectly to the distance of the oxygens in the potassium filter. When a potassium ion passes the filter pore its hydrate shell is transiently replaced by the oxygens of the amino acids in filter region. This process is energetically inert. Other ions, like sodium ions have a different sized hydrate shell radius. Stripping of the water molecules is in the case of sodium energetically not preferred and therefore entering the filter is not possible (MacKinnon 2004). B) Structure of the selectivity filter in KcsA. The five occupy sites S₀-S₄ could be alternately occupied by water molecules or potassium ions. The oxygens are orientated into the pore (Rowley & Roux 2013).

is part of the selectivity filter which is located in the tightest region of the pore. By building a fine waterway between the water filled cavity and the cell environment, this small filter allows potassium ions a fast transport over the membrane near the free diffusion rates of ions in water (Hille 2001). Not the functional groups as you could expect form the filter, the carbonyl oxygens are together with the sidechain of the threonine responsible for that. These oxygens could mimic the oxygen of the water molecules in the hydrate shell and allows to wipe off the hydrate shell from the potassium ion **Figure 2**. This nude ion is now small enough to pass the pore. A smaller ion for example sodium could not pass through this filter, because with its hydrate shell it is too big to pass. Wipe off its hydrate shell couldn't happen because the smaller size of the ion and the different distances in the hydration shells did not allow that the filter oxygens can mimic the hydrate shell. (MacKinnon 2004; Rowley & Roux 2013)

1.3.1. Modularity

Potassium channels, especially of the simple type are often used as base for artificially receptor or channel design. By coupling these basic channels to other domains, they can become gated by them. The simple composition of these channels enables a high modularity in artificial channel design. The possibility to couple the basic channels with specified gating domains is an often-chosen approach in biological sensor construction.

In the beginning of the potassium channel engineering domains like the voltage sensor domain of 6 TMD channels were fused to 2 TMD channels to show that a general exchange of parts between different potassium channels is possible (Patten et al. 1999). These works were the first hints for modularity in potassium channel. Four years later the voltage sensing domain of a phosphatase was used to gate a potassium channel (Arrigoni et al. 2013). This work showed that not just an exchange between different potassium channel domains is possible, even an exchange between different protein families is possible. The possibility to gate a potassium channel via a voltage sensor domain of a phosphatase demonstrates a general modularity of potassium channels. Further examples for the multifunctional modularity are constructs of calcium gated or even a light gated potassium channel. (DiFrancesco et al. 2015; Cosentino et al. 2015). Both channels were constructed on the base of a Kcv channel and strength the idea of Kcv as a basal building block for new biological sensors.

1.4. *Chlorella* virus potassium channel (Kcv)

Kcv channels (potassium channel out of *chlorella virus*) are a group of potassium channel out of viruses infecting *chlorella* algae. These tiny channels are diverse in their sequence and show a great structural homology to eukaryotic potassium channel. Kcv channels are the smallest known potassium channels and they are part of the 2 TMD potassium channel class. The Kcv family is divided in 2 subgroups. The KcV_{ATCV-1} (*Acanthocystis turfacea chlorella virus*) consists only of 82 amino acids distributed in two TM and the pore loop. The KcV_{PBCV-1} (*Paramecium bursaria chlorella virus*) like channels have 94 amino acids and an additional helix called slide helix. This slide helix is located at the inner part of the cell membrane and could be used as a linker to add for example a voltage sensor domain in chimeras. Despite of their size or their subgroup they own all major features of potassium channel. For example, they show a high selectivity for potassium over other ions like sodium or the typical gating of potassium channels. These minimal channels could also be inhibited by characteristic potassium channel blockers like barium (Ba²⁺).

1.5. Prokaryotic substrate-binding proteins

Substrate binding proteins were first identified as part of the ABC-transporter uptake system in prokaryotes (Kalckar 1971). Despite their diversity in sequence, a structural similarity could be observed between all binding proteins. All substrate binding proteins consist of two lobes connected by a hinge. Between these two lobes there is a binding site for the corresponding substrate (Quioco & Pflugrath 1980; Mowbray & Petsko 1983). This could be a sugar, an amino acid or even just an ion. When the substrate binds between the two lobes, a closed form of the structure is stabilized and the lobes close. The substrate is trapped between the lobes. The bound substrate can now be taken up via the ABC transporter uptake system (Berntsson et al. 2010). Structurally, the substrate binding protein is very similar to ligand binding domains of glutamate receptors, for example (Krieger et al. 2015). These also have a clamshell structure and bind a substrate between two lobes. However, this is not absorbed but leads to the stabilization of the closed structure and the resulting change in structure leading to the opening of a pore (Sobolevsky et al. 2010).

1.6. Glutamate receptor

Glutamate receptors are part of the nervous system and therefore mainly prominent in the mammalian brain. Glutamate receptors can be divided into two groups, the ionotropic (iGluRs)

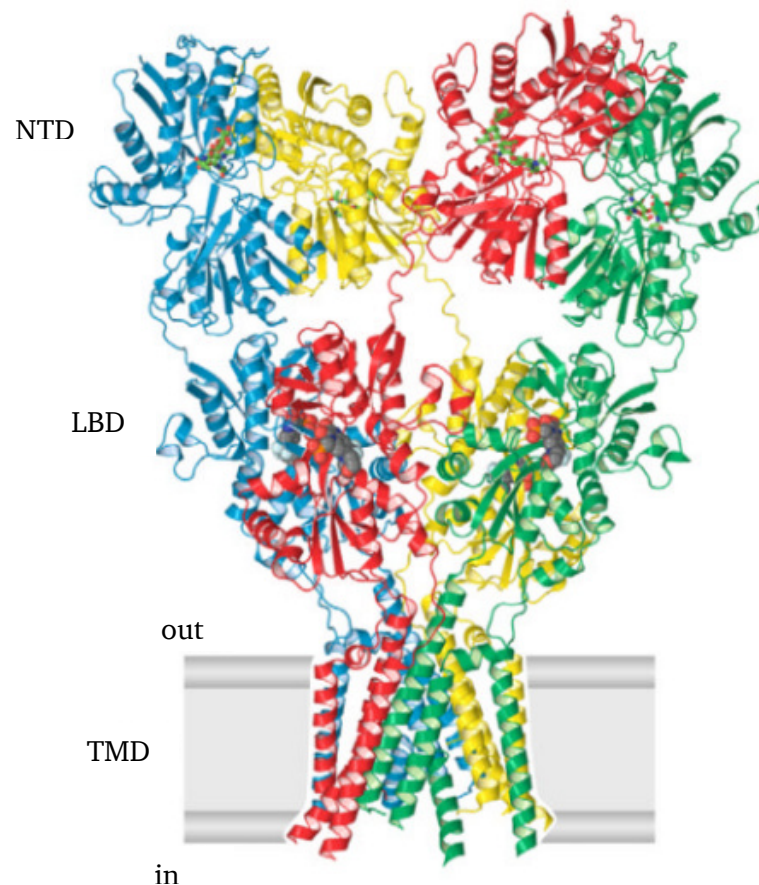


Figure 3 Structure of the AMPA GluA2. GluR are composed of three domains, representative shown by the AMPA GluA2 structure. The four subunits are colored in blue, red, yellow and green. You can see the extracellular NTD (n-terminal domain) connected through a linker to the LBD (ligand binding domain). The LBD is coupled to all three membrane spanning domains of the TMD (trans membrane domain). (Sobolevsky et al. 2010)

and the metabotropic group (mGluRs) (Dingledine et al. 1999). mGluRs are G-protein coupled receptors which activate intracellular signal cascades by activating a second messenger mechanism in consequence of the activation by glutamate. iGluRs, in contrast, fulfill after glutamate binding a structural rearrangement which leads to the opening of a pore and allows ions to pass the membrane. The iGluRs mediate the excitatory transmission in mammalian brain which is necessary for learning or memory formation (Kandel et al. 1995). The three subgroups of iGluRs are AMPA, Kainat and NMDA type receptors which are named after the glutamate analogue which opens them, too. About the forth subgroup the delta receptors not much is known until now. AMPA and Kainat receptors are often summarized as non-NMDA receptors

(Table 1). These are permeable to potassium (K⁺) and sodium (Na⁺) ions in contrast NMDA receptors are more permeable to calcium (Sobolevsky 2015). Even though the GluRs differ in

Table 1 Human and non-human (HUGO) names of glutamate receptors (Stephen F Traynelis et al. 2010):

	IUPHAR Name	HUGO Symbol	Common Names	Human Chromosome	Amino Acids in Longest Splice Variant
AMPA	GluA1	GRIA1	GluR1, GluRA	5q31.1	906
	GluA2	GRIA2	GluR2, GluRB	4q32-q33	901
	GluA3	GRIA3	GluR3, GluRC	Xq25-q26	894
	GluA4	GRIA4	GluR4, GluRD	11q22	902
Kainat	GluK1	GRIK1	GluR5	21q22.11	918
	GluK2	GRIK2	GluR6	6q16.3-q21	908
	GluK3	GRIK3	GluR7	1p34-p33	919
	GluK4	GRIK4	KA1	11q22.3	956
	GluK5	GRIK5	KA2	19q13.2	981
NMDA	GluN1	GRIN1	NMDAR1, NR1, GluRε1	9q34.3	938
	GluN2A	GRIN2A	NMDAR2A, NR2A, GluRε1	16p13.2	1464
	GluN2B	GRIN2B	NMDAR2B, NR2B, GluRε2	12p12	1484
	GluN2C	GRIN2C	NMDAR2C, NR2C, GluRε3	17q25	1236
	GluN2D	GRIN2D	NMDAR2D, NR2D, GluRε4	19q13.1-qter	1336
	GluN3A	GRIN3A	NR3A	9q31.1	1115
	GluN3B	GRIN3B	NR3B	19p13.3	1043
	GluD1	GRID1	δ1, GluR delta-1	10q22	1009
	GluD2	GRID2	δ2, GluR delta-2	4q22	1007

their kinetic and pharmacology they are all constructed in the same way (Figure 3). They consist of an extracellular region separated in two domains the NTD (n-terminal domain) and the LBD (ligand binding domain). The TMD (transmembrane domain) anchors the receptor into the membrane and allows by structural changes the pore opening and ion flux. The pore building part of iGluRs is often compared to an inverted potassium channel because of some structural mutualities. Intracellularly located is the c-terminal domain of glutamate receptors (Stephen F Traynelis et al. 2010). The NTD is with its size of around 400 AA ca. 100 AA bigger than the LBD. Whereas at the LBD ligands like glutamate, AMPA or NMDA can bind to open the pore by a structural reorganization the NTD task is resolved for NMDA receptors only. In NMDAR the NTD regulates the open probability and deactivation in addition it is involved in the allosteric receptor modulation (Furukawa 2012).

1.7. Classes of GluRs

There are three classes of glutamate receptors the AMPA, Kainat and NMDAR. AMPA and Kainat are able to build homo tetramers in heterologous expression systems while NMDA receptors need hetero tetramers to build functional structures. Because of the difficult differentiation between AMPA and Kainat receptors these two groups are often summarized as non-NMDA receptors. Both AMPA as well as Kainat receptors are mainly involved in the fast-excitatory transmission between synapses and are required for a pre-depolarization of the membrane potential to release the magnesia block in NMDA receptors.

1.8. Activating mechanisms in AMPA receptor

The LBD is the important part for receptor activation in AMPA receptors. The activation cycle starts with an unbound receptor in the inactive resting state (**Figure 4**). The initial step in the

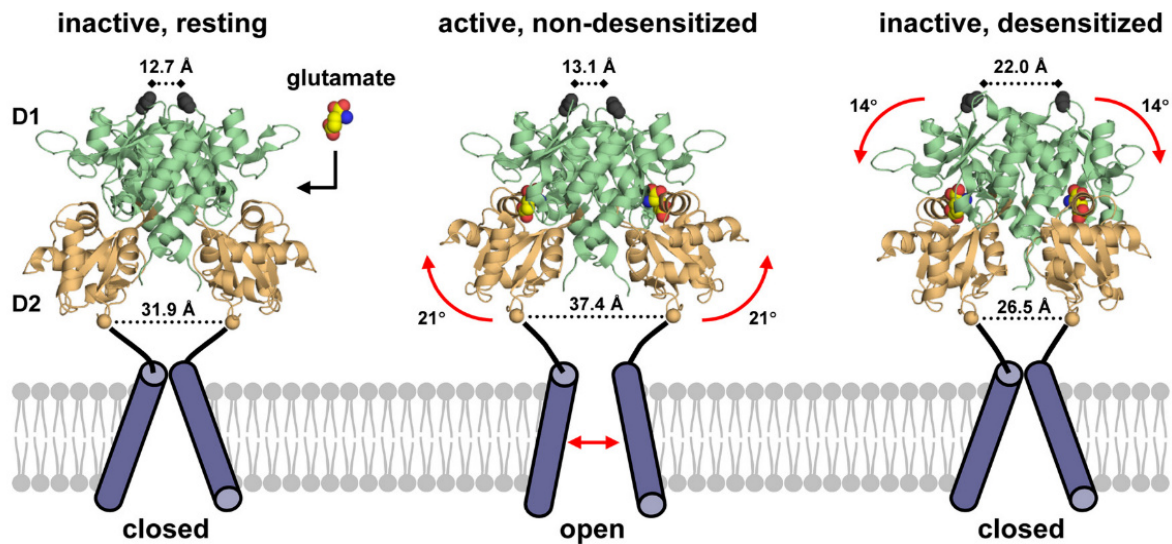


Figure 4 Conformational changes while the activation and inactivation of AMPA receptors. (Stephen F Traynelis et al. 2010) In the inactive, resting state the pore is closed and the clamshell consisting out of D1 and D2 lobe is open. Glutamate can enter the ligand binding domain (LBD) between the D1 and D2 lobe. In the active, non-desensitized state the D2 lobe flip upside to catch the glutamate. By this closing of the clamshell structure the pore gets open. In the inactive desensitized state, the dimer interface is rearranged and the complete LBD flips down. In the desensitized state the receptor pore is at least partly closed despite glutamate binding.

activation is binding of glutamate between the two LBD lobes D1/D2. The glutamate binding leads to a closure of the clamshell like structure. To occupy this conformational change after glutamate binding different crystal structures with and without bound agonist and antagonists could be compared. The comparison of those structures shows a closed clamshell with bound agonist and in contrast to a more open structure in an antagonist bound or unbound conformation. Hence, the receptor activity depends on the degree of domain closure (Armstrong & Gouaux 2000). With the closure the D2 lobe moves in the direction of the D1 and pulls the linkers coupled to the TMD out of the pore. This stretching of the linkers results in an opening of the pore and also to an instability at the TMD and LBD region which can be restored on the one hand by the reopening of the LBD interface and on the other hand by a rearrangement of the dimerization interface. With the reopening of the interface the clamshells dissociate and the agonists can leave the binding pocket. The channel closes and enters the inactive resting state again. While the rearrangement of the dimerization interface the connection between the

clamshells at back of the two binding pockets rearrange and allow the receptor to enter a desensitized conformation. In this conformation the ion conductive pore is like in the inactive state closed. Dissociation of the agonist and rearrangement of the dimer interface allows the receptor also to reach the inactive, resting state. A new binding and opening can start.

1.9. Role of NTD and TMDc in GluRs

The task of the NTD of GluRs is not completely resolved until now. From NDMAR it is known, that some small compounds can act as allosteric modulators by binding to the NTD. Some compounds which are bound by the NTD of NMDAR are zinc, protons or GluN2B selective antagonists such as Ifenprodil or Ro-25–6981 (Wilcox & Hirshkowitz 2015). In AMPA receptors especially GluA2 the NTD interacts with the N-cadherin, this synaptic complex seems to stimulate presynaptic development and function as a promoting dendritic spine formation factor (Saglietti et al. 2007). The deletion of the NTD in AMPA receptors leads to a changed desensitization and a lower surface expression but does not influence the channels in their general function (Pasternack et al. 2002). Deletion of the NTD in NMDAR showed a decreased ethanol inhibition (Wilcox & Hirshkowitz 2015). In contrast to the NTD which could be deleted without strong influences on receptor function the deletion of the M4 leads in all iGluR to a strong disability. From studies on NMDAR it is known that deletion of the M4 disturbs the channel function. The assembly or the cell surface transport is not influenced at the same time and coexpression of the M4 can recover the receptor function (Schorge & Colquhoun 2003). In contrast AMPA receptors lacking the M4 are not expressed to the cell surface (Salussolia et al. 2011). It could be shown that the M4 lacking AMPA receptor are retained in the endoplasmic reticulum. There is no tetramerization in homo- or heteromeric receptor. iGluR consists out of dimers of dimers, meaning two subunits build a dimer and two dimers assemble to a tetrameric receptor. AMPA receptors lacking the M4 seems to dimerize but these dimers will not assemble. Hence, the M4 seems to be essential in the dimerization to tetramer transition in AMPA receptors (Salussolia et al. 2013).

1.10. The relation between iGluR and potassium channel

The resemblance of iGluRs and potassium channel in their structure and sequence is pronounced in many publications. Especially the TMD without the M4 represents a potassium channel pore perfectly. A homology alignment between the GluA2, the structure model potassium channel KcsA and the in this work used potassium channel Kcv_{ATCV-1} is shown in

Figure 5 B and C. The pictogram in **Figure 5** shows the greatest differences between both types. Potassium channels are orientated in an inverted direction into the membrane in

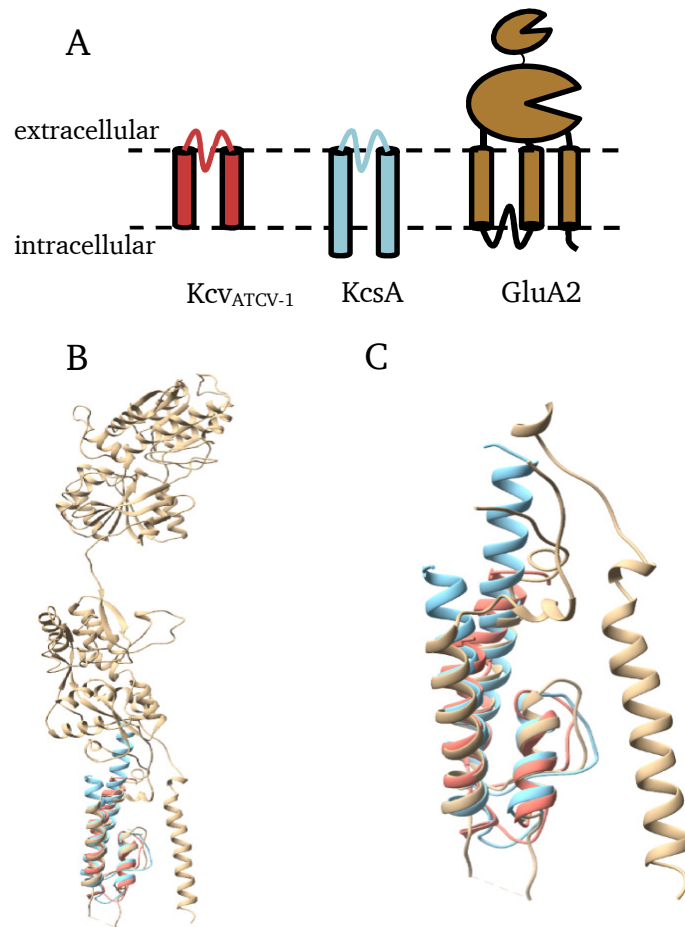


Figure 5 Structure of KcvATCV-1 (red), KcsA (blue) and GluA2 (brown). A) Pictogram of the orientation of potassium channel KcvATCV-1, KcsA and the glutamate receptor GluA2. B) Complete subunit of GluA2 (3KG2) with NTD and LBD. The KcvATCV-1 (homology model generated with swiss model) and KcsA (2HVK) are structural aligned in the TMD C) Zoom in the TMD of the three channels with the structural overlay of GluA2 against the two-potassium channel KcsA and KcvATCV-1. The channels show a strong structural similarity.

comparison to iGluRs. The pore loop is located to the outside in potassium channels and to the inside in iGluRs. The difference between KcvATCV-1 and KcsA is except of the sequence, the length of the TMD. As said before a second difference is the third TMD of GluRs. This leads to an intracellular c-terminus and an extracellular located n-terminus while in potassium channel both termini are located inside. Another hint for this relation was given by the discovery of GluR0. The bacterial GluR0 receptor was found in *Synechocystis* and is with its structure a connection between both (Chen et al. 1999). Its transmembrane region consists of just two TM without a M4. This only two TM spanning region looks like an inverted potassium channel. Interestingly in contrast to all other iGluR the GluR0 is selective for potassium. Previous

experiments, trying to change the iGluRs into potassium selective ones, no matter if the pore is exchanged or only a filter sequence is introduced, failed. Just a chimera out of mammalian iGluR and the pore of GluR0 results in a potassium selective mammalian like iGluR.

1.11. Aim of this work

In this work I want to construct an ionotropic glutamate gated potassium channel by exchanging the pore domain of GluA1 with the pore of Kcv_{ATCV-1}. This chimeric receptor would be another hint for the hypothesis that the mammalian glutamate receptors are related to potassium channel and are evolved out of a fusion between potassium channel and substrate binding proteins. In the first part the different orientation between potassium channel and glutamate receptors is addressed. An attempt is made to change the orientation of a potassium channel so that it corresponds to the orientation in a glutamate receptor. In the second part the pore of a glutamate receptor should be exchanged to build a functional and potassium selective glutamate receptor. In the third part this receptor will be minimalized to investigate the necessity of other parts than the pore or LBD for the functionality of this chimera.

2. Material and Methods

All chemicals were purchased from Sigma (Taufkirchen, Germany). NEBuilder is purchased from NEB (New England). Enzymes like Phusion polymerase are purchased from ThermoFischer (Waltham, USA).

2.1. Cloning and mutagenesis

Project I

The DNA sequence of KcV_{ATCV-1} was inserted in the multiple cloning site of vector pEGFP (Clontech, Mountain View, CA) and was kindly provided by Gerhard Thiel. The pEGFP contains a kanamycin resistance and an enhanced green fluorescent protein (EGFP) coupled with a linker directly to the protein of interest. To insert the two different signal peptides the vector was linearized by PCR with the KcV_{ATCV-1} lin. fw and KcV_{ATCV-1} lin. rw primer (Supplement 1) in a linearization PCR (polymerase chain reaction). For this 20 pmol (ca 60 ng) of plasmid was mixed with 10 pmol of each primer and a dNTP mix (dATP; dCTP; dTTP; dGTP) each 10 mM with 1 x HF Phusion buffer and 1 U Phusion DNA polymerase in a volume of 25 μ l. The PCR starts with a primary denaturation step at 98 °C for 30 seconds and then 30 rounds of 10 s denaturation at 98°C, 30 seconds annealing with an annealing temperature of 52°C and an elongation for 2 min at 72°C. A last elongation step with 1 min at 72°C ends the PCR.

The signal peptides of human-leucocyte-antigen A class1 (HLA) uniprot: P01891, β -adrenergic receptor from hamster (β) uniprot: P04274 and the trans golgi network specific integral membrane protein TGN38 of rat (TGN38) uniprot: Q63575 was used in this work. The sequence of the signal peptides was ordered as two single stranded oligonucleotides (Supplement 1) one the template and one the non-template strand and an overhang to both sides of the linearized vector. These two strands were annealed by using 200 pM of both in 50 μ l 1x PNK buffer, heated for 10 min to 95°C and then incubated at room temperature until it was cooled down. The annealed oligo was directly used with the linearized and purified plasmid in a Gibson cloning assembly with the NEBuilder according to manufacturer's manual. 25 μ M (ca. 5 μ l) of the Gibson cloning reaction was transformed into chemically competent *E. coli* by heatshock at 42 °C for 50 s. Afterwards *E. coli* were incubated on ice for 5-10 min. The *E. coli* were shaken at 500 rpm in 700 μ L antibiotic free LB medium at 37°C for 30 minutes before being plated on kanamycin (50 μ g/ml) LB-Agar plates.

After 24 hours incubation at 37 °C three colonies of each plate were picked and transferred to 20 mL LB medium with kanamycin (50 μ g/ml) and shaken with 200 rpm for 12 – 16 hours overnight. The plasmid was extracted by GenElute™ Plasmid Miniprep Kit of Sigma Aldrich.

Typically, an amount of 30 μg plasmid DNA could be extracted. The obtained plasmids were sequenced at Seqlab (Göttingen) to confirm successful insertion of desired signal peptides. Myc-tags were added in by site directed mutagenesis with extension primers (Supplement 1) following the same protocol as described above. To be sure that the signal peptide will not be read over, the start codon methionine of the KcV_{ATCV-1} is exchanged in the signal peptide constructs by a glycine by side directed mutagenesis. In these constructs only the methionine of the signal peptide can start the translation. To confirm the exchanges plasmids was sequenced at Seqlab (Göttingen).

Project II/III

R. norvegicus GluA1 glutamate receptor carrying the mutation L479Y (Genebank ID EDM04494.1) provided by R. Sprengel (MPI for medical research, Heidelberg) and the K⁺ channel from chlorella virus KcV_{ATCV-1} (GeneID 5470584) were subcloned into the expression Vector pEXP5-NT/ TOPO by using the pEXP5-CT/TOPO ® TA Expression Kit of Invitrogen. The GluATCV constructs were generated by replacing the nucleotide sequence encoding amino acids 538 to 629 (GluATCVlong), 634 (GluATCVshort) and 642 (GluATCV) of the mature GluA1 by the KcV_{ATCV-1} sequence with the use of XhoI and NheI. The GluATCV^{ΔNTD} and GluATCV^{ΔM4} constructs were generated by excising the nucleotide sequence encoding amino acids 19 to 394 and upstream of 784 of the mature GluA1 by deletion PCR, respectively. For the NTD truncated mutant the amino acids between G18 (last AA of the GluA1 signal peptide) and A395 (part of the end of the NTD). For the truncation of the M4 all AA upstream N783 (with NTD deletion N407) was deleted. The cysteine mutants were introduced by site-directed mutagenesis at position N407 (last AA when M4 is deleted) and V152 (part of the LBD TM1 linker) and confirmed by sequencing at Seqlab, Göttingen. All constructs were confirmed by DNA sequencing (Seqlab, Göttingen, Germany).

2.2. Cultivation and transfection of HEK293 cells

Human embryonic kidney (HEK293) cells were grown in T25 flasks with 5 ml MEM (minimal essential media) containing 10% FCS and 2 % Pen/Strep to a confluence of 80 to 90 %. After reaching a confluence of around 90 % the cells were harvested for transfection. For splitting the cells were washed with 2 ml PBS and then treated with 1 ml of Accutase at 37 °C for 5 min. The superseded cells were then resuspended in 5 ml media and 1/5 diluted in a new T25 flask with 5 ml media. If the cells were transfected PBS instead of media was used for resuspending and the cells were centrifuged for 2 min at 1000 rpm. The PBS was discarded and the cells resuspended in electroporation buffer with 10000 cells/ μl .

For transfection 100 μl of the cell suspension were added to the electroporation cuvette and 1000 ng plasmid were also added to the cuvette. The loaded electroporation cuvette was put into the Amaxa Nucleofector II and transfected with the program HEK293(DMSZ). After the electroporation 1 ml MEM media was added to the cells and either 100 μL was filled into 6 channel IBIDI μ -slide, for immune fluorescents staining, or into a 3 cm dish for patch clamp recordings. Cell culture dishes were coated previously with poly-d-lysine for 30 min at 37 °C.

2.3. Immunofluorescence staining

Transfected were washed two times with PBS to remove dead cells and impurities. Cells were fixed for 20 min with 4 % PFA at room temperature. For permeabilized samples, cells were permeabilized with 0.1 % Triton X-100 in 1x PBS for 10 min, non-permeabilized samples were stored in PBS for the same time. After that both permeabilized and non-permeabilized samples were washed two times with PBS and then blocked for at least 1 hour at room-temperature with block-buffer (0.5 % goat serum, 0.5 % BSA and 0.05 % gelatin in PBS). Then the samples were washed two times with PBG (PBS with 0.05% gelatin) and incubated with the primary antibody (C-Myc, DSHB, Iowa) 1:50 in antibody-buffer (5 % goat serum and 0.05 % gelatin in PBS) over night at 4 °C. The next day the cells were washed 3 times with PBG for 10 min each step. Now the second antibody Alexa 594 (Thermo Fischer) was incubated 1:400 in antibody-buffer for 1 h at room-temperature. In a last step the samples were washed 2 times with PBG, and Höchst 33342 was added.

The monoclonal antibody c-Myc (9E 10) developed by J.M. Bishop was obtained from the Developmental Studies Hybridoma Bank, created by the NICHD of the NIH and maintained at The University of Iowa, Department of Biology, Iowa City, IA 52242.

2.4. CLSM

The stained cells were imaged by a Leica TCS SP5 CLSM with 20 pictures per stack with 0.6 μM steps in z-axis with the LAS AF software of Leica (Wetzlar). For Höchst33342 staining it was stimulated with 405 nm. For GFP the stimulation was done by an argon-laser and for stimulation of TexasRed a HeNe594 laser was used. All lasers were set to 20 % intensity and the emission filter was set to 525 nm for GFP, 617 nm for TexasRed and 421 nm for Höchst33342 staining. Maximum projections of each stack were done by Fiji z-Project plugin. GFP expressing cells were edged by hand and integrated density of each channel was measured. Background fluorescence was determined by measuring non GFP expressing cells in all

channels. This background was subtracted from the density values measured at GFP expressing cells. For each condition 10-15 cells were analyzed in 3 independent stainings.

2.5. Patch clamp recordings

For electrophysiological analyses cells were used 1 day after transfection. The media was exchanged for the bath solution containing 50 mM KCl; 10mM HEPES; 1.8 mM CaCl₂; 1 mM MgCl₂; 200 mM Sucrose pH 7.4 with KOH. A glass pipette was pulled using the two-step vertical pipette puller of Narishige with the heater settings first step 64 and second step 55. This leads to a pipette with a resistance of around 12 Ω . The pipette is filled with a solution containing 110 mM KCl; 10 mM NaCl; 20 mM EGTA; 10 mM HEPES pH 7.4 with KOH. After attaching the glass-pipette to the cell membrane and breakthrough by pressure change a stimulation protocol was applied. The whole cell recordings were performed at room temperature with an L/M-EPC 7 amplifier from List Medical Electronic, Darmstadt (Germany), digitized with an analog digital converter INT-20x from NPI electronic, Tamm (Germany), at 3.57 kHz and recorded with winWCP V4.8.6 from Strathclyde Electrophysiology Software, University of Strathclyde.

The protocol shows a holding voltage of -80 mV for 200 ms then a 1s long stimulation from -140 to 140 mV in 20 mV increasing steps and 300 ms with -80 mV again.

2.6. Oocyte expression and TEVC

cRNAs were synthesized by using the AmpliCap-Max™ T7 High Yield Message Maker Kit of Cellscript (Madison, WI, USA) with the plasmid linearized by AatII. *X. laevis* oocytes were used for two electrode voltage-clamp (TEVC) electrophysiology as previously described (Lynagh et al. 2013) and under approval of the Technical University of Darmstadt (Agreement V54-19c20/15 DA8/Anz. 20). For electrophysiological analysis, oocytes were injected with 50 ng in a volume of 50 nl of the respective construct. After injection the oocytes were incubated in ND-96 solution (96 mM NaCl, 2 mM KCl, 1 mM CaCl₂, 1mM MgCl₂, 5 mM HEPES, pH 7.4 with NaOH) at 18°C for 3-5 days until the electrophysiological measurements. The TEVC recordings were performed at room temperature with an Axoclamp 900A amplifier, digitized with a Digidata 1550A at 5 kHz after low-pass filtering at 200 Hz and recorded with Clampex 10.7 (Molecular Devices, San José, USA). For recording the microelectrodes were filled with 3 M KCl (resistance 0.8 – 2.8 M Ω in external solution) and the oocytes were clamped at -70 mV. The external solution was a modified ringer solution containing 100 mM KCl; 10 mM HEPES; 1.8 mM CaCl₂; 1 mM MgCl₂ (pH 7.4 with KOH) alone or containing agonist. L-glutamate, CNQX and Ba²⁺ were applied to the oocytes in external solution at the given concentrations. Dose-

response curves of CNQX were determined in the presence of 5 μ M glutamate (corresponding to the EC₅₀ value) and normalized to the current in the absence of CNQX. Whole-cell current-voltage relationships of saturating glutamate-induced currents were recorded in ramps from -140 mV to 140 mV with 14mV/100ms in 2 s in solutions with different concentration of potassium (substituted by sodium) and corrected by the current values obtained in the absence of glutamate. For treatments with dithiothreitol (DTT), oocytes were superfused with 2 mM DTT for 100 s before applying glutamate in the presence of 2 mM DTT as described by Lynagh et al. (2013)(Lynagh et al. 2013).

2.7. Protein production and Bilayer measurements

The proteins of Kcv_{ATCV-1} and Kcv_{ATCV-1}^{*} were produced in an in vitro transcription reaction with the MembraneMax™ HN Protein Expression Kit in presence of nanolipoproteins in accordance with manufacturer`s instructions (Winterstein et al. 2018). The reaction was purified by His-tags fused to the nanolipoproteins over a HisPur NI-NTA spin column (Thermo Scientific, Waltham, USA) after manufacturer protocol and eluted with 250 mM imidazole. For bilayer experiments a dilution of 1:5000 in 250 mM imidazole was used.

Bilayer experiments were performed in a vertical planar lipid bilayer chamber (Winterstein et al. 2018) and channel activity was measured with an eOne Amplifier from Elements s.r.l., (Cesena, Italy) under symmetric conditions with solution containing 100 mM potassium chloride with 10 mM HEPES pH 7.4. Planar lipid bilayers were formed over a hole of ca. 100 μ m in a 20 μ m Teflon foil, which was pretreated with 1% hexadecane solution in n-hexane. Bilayers were made from 1,2-diphytanoyl-sn-glycero-3-phosphocholine (DPhPC, from Avanti Polar Lipids, Alabaster, Alabama) diluted at 15 mg/ml in n-pentane with the folding technique (Montal & Mueller 1972). The phospholipid solution was therefore added as monolayer on the measure solution and after evaporation of the solvent a bilayer was folded by raising the solutions in the chambers. After formation of a bilayer, the electrical activity of the empty membrane was monitored at a voltage of \pm 100 mV to exclude contaminations or lipid pores. Only when the bilayer was stable and electrically silent a small amount (1 μ l) of protein (Kcv_{ATCV-1} or Kcv_{ATCV-1}^{*}) in nanodiscs diluted 1:5000 in 250mM imidazole was added to the trans chamber near the membrane with a Hamilton syringe. After insertion of an active channel the voltage protocol was applied again and the resulting currents were recorded with Ag/AgCl electrodes. The data were digitized at 5 kHz after lowpass filtering at 2.5 kHz.

2.8. Prediction of the protein-orientation within the membrane

To predict the orientation of KcV_{ATCV-1} in the membrane without and with different signal peptides TMHMM (<http://www.cbs.dtu.dk/services/TMHMM/>; last modification Thursday 5th 2017) and Phobius (<http://phobius.sbc.su.se/>) was used. The protein sequence was load in with default settings.

2.9. Structure model

The homology model of KcV_{ATCV-1} was made with swiss-model against the KirBac1.1 (Tayefeh et al. 2009), the structure overlays was built with UCSF Chimera (Pettersen et al. 2004) and the MatchMaker plugin with default values.

The homology model of GluATCV* ΔM4 was built against the GluA2 structure 3KG2 with swiss-model and the structure overlays was built with UCSF Chimera (Pettersen et al. 2004) and the MatchMaker plugin with default values. Distance of C152/C407 mutants was measured in this homology model of GluATCV* ΔM4 by the chimera distance tool between Cα atoms.

2.10. Analysis

Current responses to glutamate were plotted against glutamate conceation and fit with non-linear regression with variable slope in Prism version 7.00 (GraphPad Software Inc., La Jolla, USA) as described (Lynagh & Laube 2014). The proportion of glutamate sensitive current to complete barium sensitive current was calculated by $I_{\text{Glu}}/I_{\text{Ba}}$. Permeability ratio was calculated by the shift of the reversal potential with the Goldman-Hodgkin-Katz equation under bi-ionic conditions $\frac{P_{\text{Na}^+}}{P_{\text{K}^+}} = \exp(\Delta E_{\text{rev}} * \frac{F}{R * T})$ (Gazzarrini et al. 2009). The amplitude was measured with KielPatch and also the open probability in bilayer measurements was analyzed by the build in Hinkley-jump-detector of KielPatch (<http://www.zbm.uni-kiel.de/aghansen/software.html>). Values given represent means ± SEM. Statistical significance was determined at the $p < 0.05$ (*), $p < 0.01$ (**) and $p < 0.001$ (***) levels using a Student's two-tailed, unpaired t-test or ANOVA (in case of more groups) and a Tukey post hoc analysis (Prism 7.00).

3. Project I - Orientation of Kcv_{ATCV-1} channel in the cell membrane of HEK293 cells

3.1. Introduction

Potassium channels are omnipresent in nearly all known organisms and involved in crucial cell functions like proliferation, energy management, communication and much more (Kuo et al. 2005; Miller 2000).

This omnipresence and diversity make them to an interesting topic for various researchers. The wide distribution through all kinds of organisms leads to the idea of a rudimentary channel type of them (Anderson & Greenberg 2001). It is a general assumption that all potassium channel follow the same structure with a pore, build of two transmembrane regions, and a pore loop containing the filter sequence, while this filter is orientated to the extracellular space (Kuang et al. 2015). Based on this assumption and the similar structure, a relation between potassium channel and glutamate receptors, as an inverted counterpart, was propagated, but not confirmed (Chen et al. 1999; Sobolevsky et al. 2003). The pore domain of both show strong similarities but the orientation in the membrane is inverted, so that if there is a relation between them an inversion, during evolution of the potassium channel, must have happened. The pore of glutamate receptors is in contrast to potassium channel pores not selective for one special ion. For example, they show a (P_K/P_{Na}) of 1.14 for NMDA and (P_K/P_{Na}) of 1.25 for AMPA and Kainat receptors, they are in fact equal (Stephen F. Traynelis et al. 2010). A rudimentary group of potassium channel the Kcvs will be used for proving if it is possible to insert a potassium channel functional in different orientations. Despite their small size of just 82 amino acids the Kcv channels show the main characteristics of potassium channel. They own a strong selectivity for potassium and the typical orientation with the filter in the extracellular side. Also, they can be blocked by typical potassium channel blockers like Ba^{2+} (Piasta et al. 2011; Armstrong & Taylor 1980). If there is a relation between GluRs, which show a similar structure, and potassium channels, an insertion in both directions should be functional. This would be a hint for a relationship between these two in different directions orientated channel families. The advantages of Kcv is their small size and their missing coevolution in this niche of chlorella virus. For the inversion of the Kcv_{ATCV-1} signal peptides will be used to push it into a defined orientation in the membrane. Signal peptides or also called topogenic sequences are short sequences of 18-40 amino acids at the n-terminus of proteins which can determine the orientation. The orientation of a protein is mostly determined during or immediately after the synthesis at the endoplasmic reticulum (Hartmann et al. 1989). Because a signal peptide is part of most membrane proteins a large selection of different signal peptides exists. To predict the orientation of a protein Hartmann et al. established 1989 a prediction system which is based

on a ratio between the n- and c-terminal region of proteins. Special amino acids got values between -1 and 1 and the ration between the n- or c-terminal region is an amount of the orientation (Hartmann et al. 1989). Today there are a couple of different prediction tools for example TMHMM (Krogh et al. 2001) or Phoebius (Krogh et al. 2004). Both work with hidden Markov models to model difference sequence regions.

Aim of this chapter is to show that it is possible to express a functional potassium channel in the same inverted orientation into a membrane as it is known from GluRs. A small potassium channel like the Kcv_{ATCV-1} which can functional expressed in two direction would be a perfect candidate for further experiments in GluR pore research.

3.2. Results

3.2.1. Influence of signal peptides to the electrophysiological response of Kcv_{ATCV-1}

To test if it is possible to insert the viral potassium channel Kcv_{ATCV-1} in an inverted orientation in HEK293 cells I used the human-leucocyte-antigen class1 (HLA) signal peptide coupled to that channel. The Kcv_{ATCV-1} is c-terminal linked to an eGFP that you can recognize Kcv expressing cells at the green fluorescence. In other studies, it could be shown that the Kcv channels are with their small size and their robust potassium permeability a perfect system for building block experiments (Arrigoni et al. 2013; Cosentino et al. 2015). The Kcv channels show their opportunity to build a great model system for the pore building region of potassium channel (Thiel et al. 2011). With their small size of 82AS in the case of Kcv_{ATCV-1} and their composition of only 2 TM per subunit and a selectivity filter they show all necessary parts of a potassium channel pore. In silico tests with TMHMM and Phoebius prediction indicate that Kcv_{ATCV-1} coupled to the signal peptide of HLA shows strong hints that coupling it to the Kcv_{ATCV-1} shows

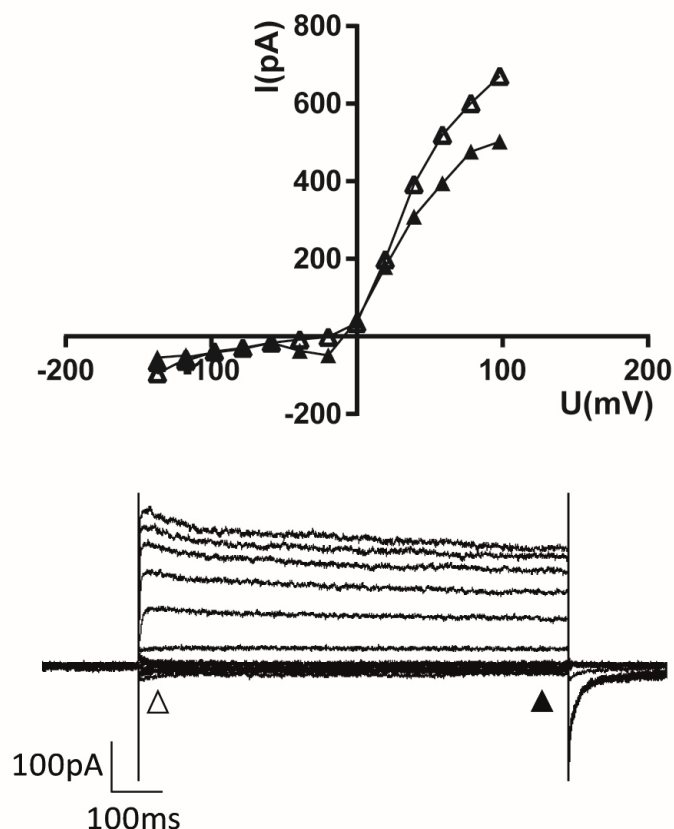


Figure 6 Patch clamp recording of an untransfected HEK293 cell. Current-voltage curve of a representing HEK293 cell. Open triangles show the instantaneous current and closed triangles show the steady state current. The untransfected HEK293 cell shows just a small influx current but a higher outward current. At the bottom you can see the corresponding current answer of a voltage protocol from -140 to 100 mV in 20 mV steps.

a different orientation than the wildtype. In a prediction without any coupled signal peptide the prediction tools showed an orientation in the cell membrane with the pore in the direction of the cell outside. Using the modification with the signal peptide results in a channel with the pore located in the direction to the cytoplasm (**Supplement 2**). To approve that prediction, I cloned the signal peptide of HLA in front of the start codon of Kcv_{ATCV-1} and changed the methionine of the Kcv to a glycine to avoid proteins expressed with a read over signal peptide. In a first step I measured not transfected HEK 293 cells as a negative control (**Figure 6**). They show no or just a weak influx and an outflux with lower than 1 μA (**Figure 6**). Because of their low intrinsic channel expression, they are a good tool for overexpressing channels or receptors and analyzing them in a robust living environment (Ooi et al. 2016).

In contrast to not transfected cells, cells expressing the Kcv_{ATCV-1} wildtype show a linear ohmic behavior but in both extremes in positive and negative voltage ranges a maximum between 80 to 110 mV is reached (**Figure 7**). The currents with more than 1 μA in the inward and outward current in transfected HEK293 cells are significantly different from wt (compare **Figure 7** and

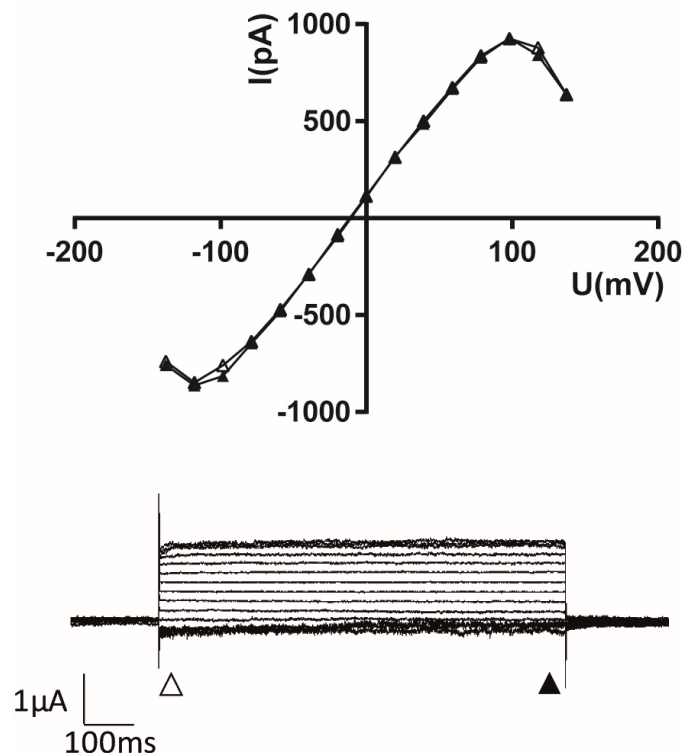


Figure 7 Representative patch clamp recording of a HEK cell expressing Kcv_{ATCV-1}. At the top: current voltage curve from a HEK293 cell transfected with the Kcv_{ATCV-1} wildtype. In both ranges positive and negative voltage, a flattened curve occurred while in the middle an ohmic resistance could be assumed. The open triangles show the instantaneous current and the closed triangles the steady-state current. At the bottom you can see the corresponding answer of the transfected cell to a voltage protocol from -140 to 140 mV with a clamp voltage of -80 mV.

Figure 6). The reversal potential of ca. -20 mV indicates potassium as the main conducted ion. The calculated reversal potential for the used pipette and bath solution is with a Nernst potential of about -20 mV for potassium really close to the measured reversal potential of -18 mV. The Nernst potential of other possible ions in the solutions are in a high distance to that potential. The instantaneous and steady state current are also similar. Because of this similarity in both the inward and outward current no great change in the current voltage curve of the inverted channel was expected.

Even more surprising HEK293 cells expressing the HLA signal peptide coupled to the KcV_{ATCV-1} (HLA-KcV_{ATCV-1}) show an answer which indicates strong influx without any flattening and a weak strongly flattened outflux similar to the outflux of the KcV_{ATCV-1} (**Figure 8**). Hence, there is a huge difference between both answers in the influx current. These differences could be a hint for an orientation in two different directions of the KcV_{ATCV-1} in HEK293 cells or maybe a changed gating by an inverted orientation into the membrane.

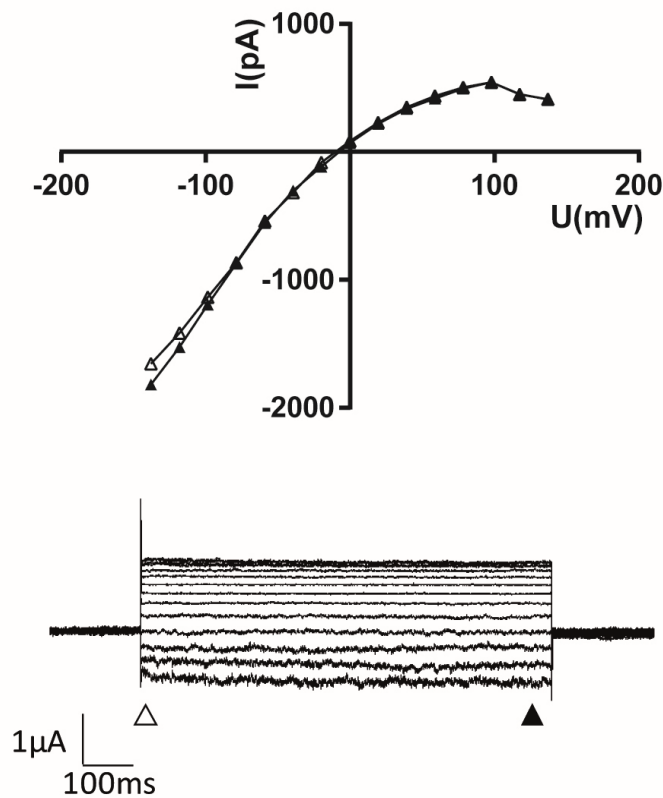


Figure 8 Representative patch clamp recording of an HEK cell expressing the HLA signal peptide coupled to KcV_{ATCV-1} (HLA-KcV_{ATCV-1}). The filled triangles show the end of the measurement with the steady-state current while the open triangles show the instantaneous current of the HLA-KcV_{ATCV-1}. In negative voltage ranges a linear inward current occurred while in the positive voltage range the outward current shows with higher voltages a flattened shape.

To verify one of these two hypotheses, I tested other signal peptides. Therefore I want to use a signal peptide which should insert the Kcv_{ATCV-1} into the same orientation as it is already orientated. If the inversion of the channel is responsible for that change in its behavior, the added signal peptide should not influence the typical Kcv_{ATCV-1} current voltage curve and should work as a negative control. If the Kcv_{ATCV-1} is normally located in both directions into the membrane an answer different to Kcv_{ATCV-1} and different to that with HLA signal peptide coupled should occur. In a first trial the signal peptide of the trans golgi network specific integral membrane protein TGN38 of rat which shows *in silico* the same orientation as the wildtype was used. The whole cell patch clamp measurements look like the HLA-Kcv_{ATCV-1} ones (**Supplement 3**). In a second trial I used for these experiments the signal peptide of the β -adrenergic receptor from hamster (β), which shows *in silico* the same orientation as the HLA. I cloned it in front of the Kcv_{ATCV-1} and also the methionine was substituted. Expression of β -adrenergic receptor-signal peptide from hamster coupled to the Kcv_{ATCV-1} (β -Kcv_{ATCV-1}) in HEK293 cells leads to a

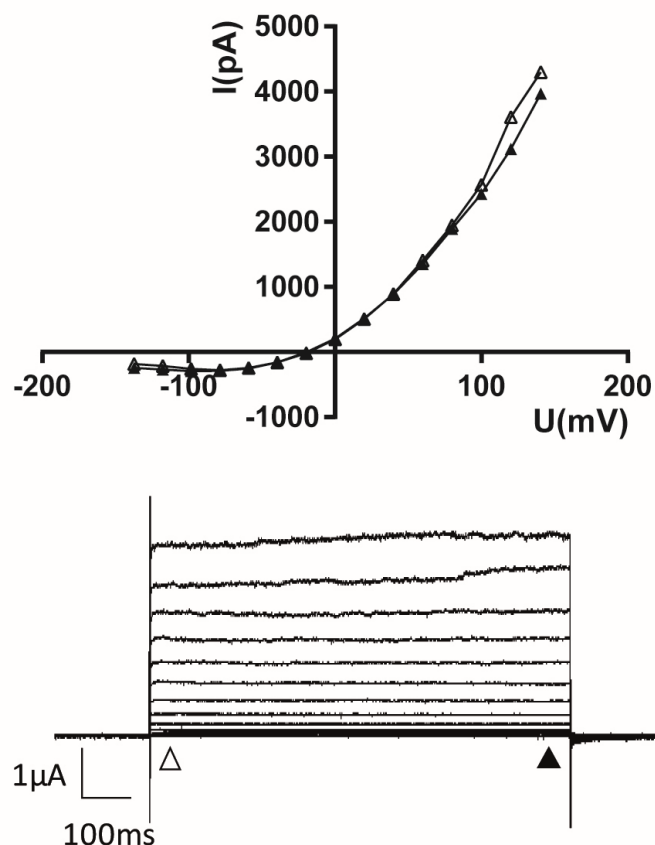


Figure 9 Representative patch clamp recording of an HEK cell expressing the β -adrenergic signal peptide coupled to Kcv_{ATCV-1} (β -Kcv_{ATCV-1}). The current voltage diagram shows a low to no influx in the negative voltage range. a strong influx occurred in the positive voltage range. The open triangles show the instantaneous current and the closed ones the steady-state current. Both are really similar to the Kcv_{ATCV-1}.

completely changed electrophysiological behavior and looks like an inverted HLA-Kcv_{ATCV-1} (Figure 9). There is a lower influx of potassium with a flattened shape like in the negative voltage range of the Kcv_{ATCV-1} but a linear outflux without any flattening in the positive voltage. Both the instantaneous and steady state currents show a similar kinetic and a reduction in the influx current comparable to the influx reduction in the Kcv_{ATCV-1}. The reversal potential of -20 mV is expected as the reversal potential for potassium as the main conducted ion within my used solutions. The current voltage curve derived from the whole cell kinetics are also similar to current-voltage curves recorded from bilayer single channel recordings of Kcv_{ATCV-1} (Rauh et al. 2017) which shows a lower current amplitude in negative voltage ranges. Therefore, you could assume that the orientation of the β -adrenergic signal peptide coupled Kcv_{ATCV-1} is similar to the one you could find in bilayer measurements. Building the mean of 7 to 13 measurements per construct shows a significant difference between the three constructs at least in the extrema of positive or negative voltages. The flattened parts of the signal peptide coupled Kcv_{ATCV-1} fits perfectly to the analogical flattened region in positive or negative voltage range (Figure 10). The influx at -140 mV of the HLA-Kcv_{ATCV-1} is significantly different to Kcv_{ATCV-1} and the β -Kcv_{ATCV-1}, which are both not significantly different among themselves. Vice versa at 140 mV

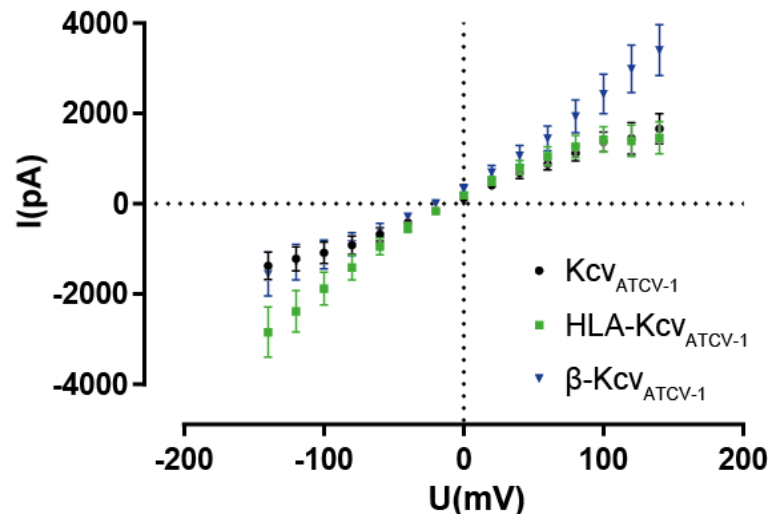


Figure 10 Overview of the 3 Kcv_{ATCV-1} constructs. The Kcv_{ATCV-1} is shown with black circles and SEM, it shows in both the negative and positive range a flattening (n=12). The HLA construct is shown in green squares with SEM (n=13) and shows just a flattening in the positive voltage which is really similar to the flattening shown by the Kcv_{ATCV-1} in this voltage area. The β -adrenergic signal peptide coupled Kcv_{ATCV-1} shown in blue triangles with SEM (n=7) has in the negative voltage range a similar flattening as the Kcv_{ATCV-1}.

the outflux of Kcv_{ATCV-1} and the HLA-Kcv_{ATCV-1} are not significantly different but the β -Kcv_{ATCV-1} is significantly different to both. Forming a rectification coefficient between -100 and 100 mV

of all measured cells shows a rectification coefficient ($|-100/100|$) of 0.74 ± 0.07 for the Kcv_{ATCV-1} , 1.33 ± 0.07 for the $HLA-Kcv_{ATCV-1}$ and 0.46 ± 0.1 for the $\beta-Kcv_{ATCV-1}$ (**Figure 11**). Using this coefficient to find a combination of both signal peptide coupled versions which shows a similar

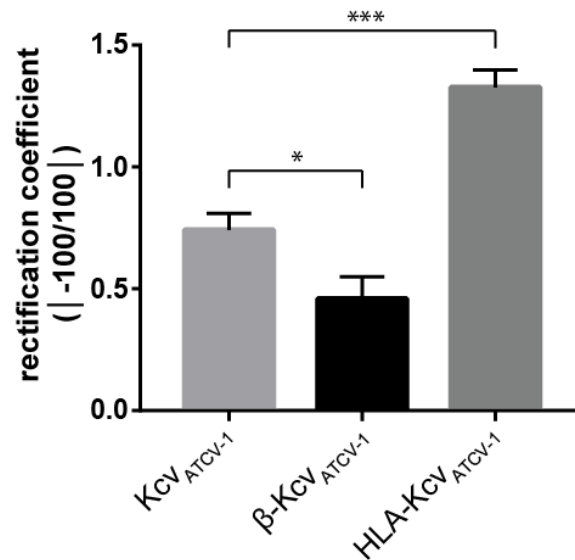


Figure 11 Rectification coefficient for the Kcv_{ATCV-1} and signal peptide coupled Kcv_{ATCV-1} . KCV_{ATCV-1} differs from both constructs. The distinction to the $\beta-KCV_{ATCV-1}$ is significant ($p=0,022$) and to the $HLA KCV_{ATCV-1}$ is highly significant ($p<0,001$). Bars show mean \pm SEM. (ANOVA and a Tukey post hoc analysis (Prism 7.00))

rectification coefficient like the Kcv_{ATCV-1} shows that I would need around 30 % of HLA and 70 % of β signal peptide coupled channels for a coefficient of 0.74. While different orientations of these three constructs could be deduced from the different electrophysiological answers. It looks like the Kcv wildtype without signal peptides could be inserted in the membrane in both directions indicated by the flattened answer in both, the inward and the outward currents. The two constructs with signal peptide show each in one extreme a flattened current. Therefore, maybe the wildtype could also be a combination of these two orientations. Because of this indication of the possible two directions for the Kcv_{ATCV-1} orientation and the inexact seeming orientation-prediction I want to check these within a direct proof of the orientation.

3.2.2. Determination of the channel orientation of Kcv_{ATCV-1} by immunostaining

To determine the orientation of the Kcv_{ATCV-1} with and without signal peptides I used an immunostaining approach. Therefore, I coupled the eGFP construct with an additional Myc-Tag to address the location of the tag with immunostainings. To differentiate the two possible

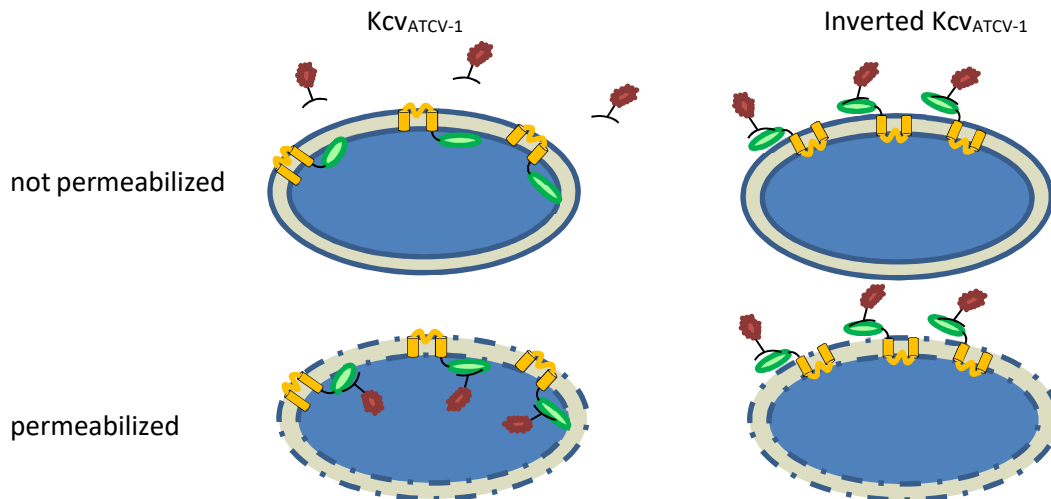


Figure 12 Strategy for detecting the direction of the Kcv_{ATCV-1}. The channel is coupled with the eGFP and the Myc-Tag. The Myc-Tag antibody (red) recognises the Myc-Tag (green) of each Kcv_{ATCV-1} subunit (orange). If the Membrane is intact (top) the antibody can only detect Myc-Tags outside the cell (right). To detected Myc-Tags inside the cell it has to be permeabilized for example by Triton-x 100 (bottom).

localizations inside and outside the cell I used a staining under non-permeabilized conditions. Only Myc-Tags which are located outside of the cell membrane could be detected in this case. If there is an in the common direction orientated channel under non permeabilized conditions the Myc-Tag should be located inside the cell and no signal should be detectable. In the case of an inverted insertion a signal from the Myc-Tag should occur because the inverted insertion leads to an outside localization of the Myc-Tag. With permeabilization conditions the cell membrane is no barrier for the antibody and in every probe a signal should be detectable (**Figure 12**). With the eGFP coupled to the protein I could differentiate between cells expressing the channel and the ones that do not. For detection under permeabilized conditions a common fluorescence microscope is used. For non-permeabilized conditions a CLSM is used because of the higher sensitivity. The images of **Figure 13**, **Figure 14** and **Figure 15** are maximum intensity projections over all images of a stack. A single image is shown in the supplements (**Supplement 4**). The fluorescence images of Kcv_{ATCV-1} under non-permeabilized conditions show just a weak signal in the Myc-Tag channel as expected (**Figure 13**). In the normal insertion direction, no Myc-Tag should be outside and therefore no signal should occur. This weak signal

could occur on the one hand from unbound antibody or from a small amount of inverse inserted channels. For quantification the integrated fluorescence for both channels (GFP and Myc) was determined. The mean of the integrated density of no GFP expressing cells was subtracted from

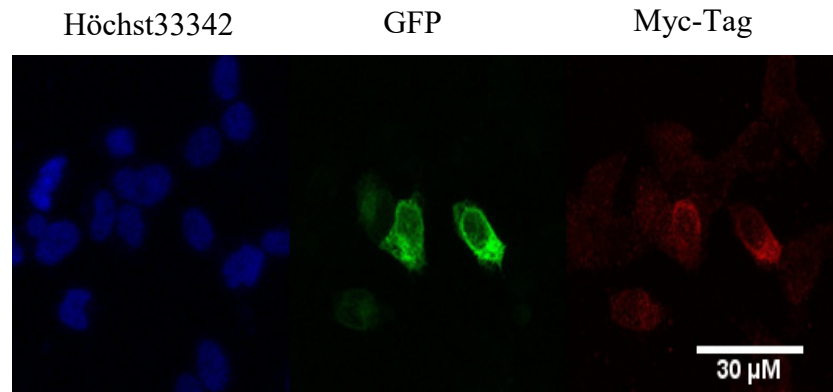


Figure 13 Maximum intensity projection of CLSM image of Kcv_{ATCV-1} coupled to eGFP (green) stained with Höchst33342 (blue) and with a weak fluorescence signal in the Myc-Tag (red) channel. Scalebar: 30 μ M

the one expressing GFP to exclude background of unbound antibody. The ratio of the fluorescence integrated density between Myc-Tag signal and the GFP signal is 0.15 ± 0.09 (**Figure 13**). Transfection of HEK293 cells with the HLA signal peptide coupled Kcv_{ATCV-1} leads to a strong signal in the Myc channel (**Figure 14**). There is also a background at no GFP expressing cells by unbound and not completely washed off antibody but the relation between

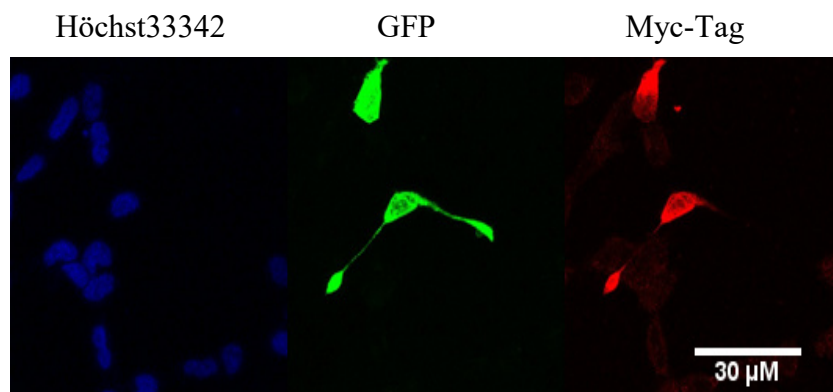


Figure 14 Maximum intensity projection of CLSM image of HLA-Kcv_{ATCV-1}. Images of three channels in coupled Kcv showing strong signal in eGFP (green) and Myc-Tag (red) channel. In blue the nuclei stained with Höchst33342. Scalebar: 30 μ M

GFP and Myc signal seems to be much higher even by eye. Quantification of the fluorescence integrated density shows a ratio between Myc signal and eGFP signal of 0.45 ± 0.06 (**Figure 16**). Kcv_{ATCV-1} coupled to the β -adrenergic-receptor signal-peptide leads to no visible signal in

the Myc channel (**Figure 15**). Quantification of the fluorescence integrated density ratio between GFP and Myc signal after background correction is only 0.02 ± 0.03 (**Figure 16**). Like

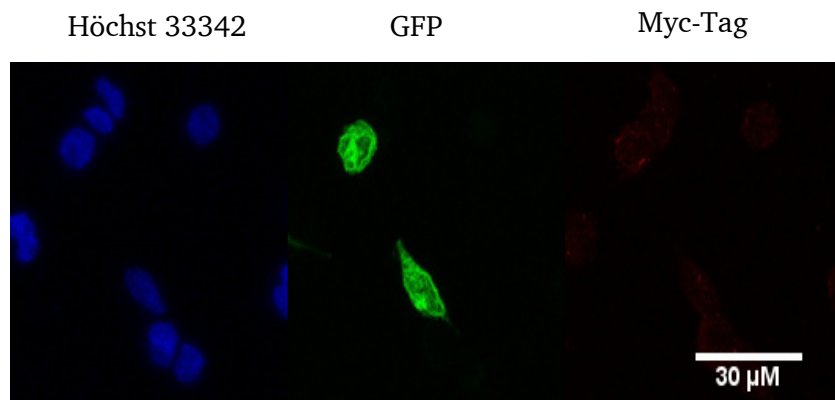


Figure 15 Maximum intensity projection of CLSM image of β -Kcv_{ATCV-1}. No signal in the Myc-Tag (red) channel but with strong signals in the eGFP-channel (green) is visible. The nuclei are stained with Höchst33342 (blue). Scalebar: 30 μ M

known from the electrophysiological data the golgi sialyltransferase coupled Kcv behaves like the HLA and therefore should have the same orientation. This result could be interpreted that there is no Myc-Tag outside the HEK293 cell and therefore no Kcv channel is orientated with its pore loop to the cytoplasm. In contrast to the Kcv wildtype without any signal peptide, where I found a gentle correlation between the fluorescent signals, the signal peptide of the β -

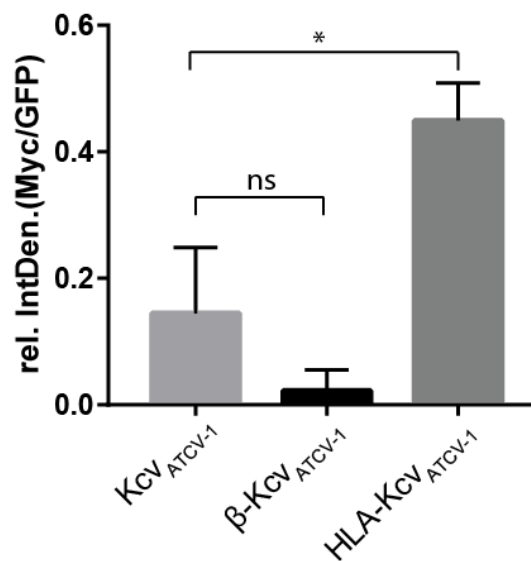


Figure 16 Fluorescence integrated density of Myc-Tag in relation to GFP signal for the Kcv_{ATCV-1} and signal peptide coupled Kcv_{ATCV-1}. The total number of cells are 30-40 cells per bar out of 3 repeats of the experiment mean \pm SEM. (0.15 ± 0.1 vs. 0.45 ± 0.06 rel.IntDen., $p < 0.033$). Note the variance of Kcv_{ATCV-1} is with 0.42 more than 3 times greater than β (0.12) or HLA (0.08). (ANOVA and a Tukey post hoc analysis (Prism 7.00))

adrenergic-receptor seems to orientate all Kcv in the normal common direction. A comparison of the different orientations in the membrane supports the idea of a change in the orientation by adding signal peptides to the Kcv_{ATCV-1}. If I assume that in the case of the β -adrenergic signal peptide all Kcv channels are orientated in the same direction and in the case of HLA all Kcv are orientated to the opposite and use both to normalize the relative integrated density ca. 30 % of the Kcv_{ATCV-1} wildtype would be orientated in the same direction as the HLA and ca. 70 % would be orientated as the with β -adrenergic signal peptide coupled ones.

3.3. Discussion

My data demonstrate that a coupling of signal peptides from different proteins or organisms to the viral potassium channel KcV_{ATCV-1} allows to define the orientation of the channel orientation in the cell membrane. By using electrophysiological and immunostaining approaches I can not only prove that the orientation of a KcV_{ATCV-1} can be inverted, further my results indicate that the potassium channel KcV_{ATCV-1} seems to insert in two different orientations into the cell membrane by its own.

It is the general opinion that all potassium channels follow not just the same blueprint but also the orientation in the membrane seems to be throughout all the different potassium channels the same (comparison with OPM database). A prediction of the orientation for KcV_{ATCV-1} with two different prediction tools shows the direction like for other potassium channels, the pore is orientated to the outer environment. The simple adding of a signal peptide of the human-leucocyte-antigen class1 (HLA) changed the orientation in the prediction to the opposite. This *in silico* prediction results have to be considered with caution as such tools are not 100% accurate and there is still a false classification (Krogh et al. 2004). Comparing these both constructs with and without an additional signal peptide in patch clamp measurements shows a completely different kinetic expressed in HEK293 cells (**Figure 7** and **Figure 8**). The KcV_{ATCV-1} shows a virtually symmetric kinetic with flattened currents in the inward as well as in the outward direction. In contrast the HLA coupled one shows just in the outward current such a flattening. These differences could occur because of multiple possibilities. For example, the added signal peptide could directly influence the channel properties not by the inverted orientation but by mechanical disorders. Using two other signal peptides results in one case, with the trans golgi network specific integral membrane protein TGN38 signal peptide, in a similar whole cell current like the HLA and in the case of the β -adrenergic receptor signal peptide coupled to KcV_{ATCV-1} in a completely inverted result (**Figure 9** and **Supplement 3**). This current of β -KcV_{ATCV-1} looks different to the KcV_{ATCV-1} and to the HLA-KcV_{ATCV-1} (**Figure 7** and **Figure 8**). The single channel measurements in bilayer (Rauh et al. 2017) and also single channel measurements made in oocytes (Gazzarrini et al. 2009) are similar and show a comparable current to the β -KcV_{ATCV-1}. Supposing that the KcV_{ATCV-1} have not just one orientation and HLA-/ β - KcV_{ATCV-1} represent each a specified orientation could be an explanation for these results.

The results of the CLSM images further support this idea. While in the case of the HLA-KcV_{ATCV-1} a strong fluorescence signal is detectable in not permeabilized cells. In the case of β -KcV_{ATCV-1} no signal could be detected. Without permeabilization, the antibodies could just detect antigens

outside the cell membrane, all other antigens inside the cell are not reachable. Because the localization of the Myc-Tag is dependent on the orientation of the Kcv_{ATCV-1} in the membrane this setup allows to directly measure the orientation within the membrane. Comparable to the electrophysiological measurements HLA- and β -signal peptide coupled constructs of the Kcv_{ATCV-1} show contrary results. While HLA coupled Kcv_{ATCV-1} show in electrophysiological measurements a flattening only in the outward current and a strong signal in the antibody staining, the β -signal peptide coupled Kcv_{ATCV-1} displays a flattening within the electrophysiological measurements only in the inward current and no to little detectable signal in the antibody staining (**Figure 9** and **Figure 15**). Both results, electrophysiological measurements as well as antibody staining suggest a different orientation of the Kcv_{ATCV-1} coupled to signal peptides. The Kcv_{ATCV-1} without any additional signal peptide shows in the electrophysiological measurements a flattening in positive and negative voltage ranges. This could happen because this is the normal behavior of this channel in this environment or because of a non-defined orientation. Because there is no potassium channel known which is orientated with its pore to the cell inside it would be logical that this current voltage behavior is regular. In contrast to this the antibody staining without signal peptide show a weaker signal indicating that a small amount of the channel is orientated with the detectable Myc-Tag to the cell outside. Quantification of the fluorescent signal indicate that around 30 % of the proteins are non-usual orientated (**Figure 16**), if you assume that in the case of the β -adrenergic signal peptide all Kcv channels are orientated to the one, and in the case of HLA all Kcv are orientated to the other direction and use both to normalize the relative integrated density. Indicated by a strong variance in the rel. IntDen. the different orientation seems to change strongly between different cells. In contrast the variance of the signal peptide coupled Kcv_{ATCV-1} are much lower. The electrophysiological measurements further support the indication of two different orientated populations of Kcv_{ATCV-1}. Set up a rectification coefficient between -100 and 100 mV allows to compare the rectification between these three constructs (**Figure 11**). Using the rectification coefficients of the signal peptide coupled Kcv_{ATCV-1} channels to calculate the amount of usual orientated channels without a signal peptide a similar result as with the antibody staining's could be produced. Again 30 % of the proteins should be orientated in a non-standard direction and 70 % should be orientated as usual.

A first indication of an inversely orientated potassium channel was the discovery of the GluR0 in 1999 (Chen et al. 1999). This bacterial glutamate receptor shows like eukaryotic glutamate receptors a structural similarity to potassium channel. They are consisting of four subunits but the pore looks like an inverted potassium channel. Because of this similarity a relation between glutamate receptors and potassium channels was hypothesized for a long time (Sobolevsky et al. 2003; Wood et al. 1995). The GluR0 receptors have a high selectivity for potassium and

consist other than eukaryotic glutamate receptors of just 2 and not 3 trans membrane domains. Even though there is a strong similarity to potassium channels it is just an indication that this receptor has evolved from potassium channels. My results show that an inversion of potassium channels is possible and therefore a necessary feature for the evolvement of the glutamate receptor derived from potassium channel is given. Furthermore, it shows that an orientation of potassium channels in an inverted direction is possible even without any signal peptide. These rudimental small potassium channels seem to be inserted in different orientations into the cell membrane and could therefore be part of an ancient group which is involved in the development of higher glutamate receptor.

4. Project II - Fusion of Kcv_{ATCV-1} with AMPA receptor - A ligand gated potassium channel chimera

Chapter II is published in the same or similar form as Schönrock et al. 2019 in communications biology.

4.1. Introduction

Conversion of a chemical to an electrical signal is a hallmark of neurons in the central nervous system (CNS). This process is mediated by different families of ligand-gated ion-channels, membrane-spanning proteins that open upon recognition of a specific neurotransmitter. In particular, gating of cation-permeable receptors by the amino acid glutamate (iGluRs) mediating excitatory neuronal signaling in the mammalian CNS is crucially involved in both, learning and memory formation and pathological mechanisms leading to excitotoxic neuronal damage in diverse neurological diseases (Stephen F Traynelis et al. 2010). Because mutations within subunits are associated with a number of diseases of the nervous system, these receptors are of interest as a major class of targets for novel drugs. The mammalian iGluR family includes three major subtypes represented by several subunits: AMPA (α -amino-3-hydroxyl-5-methyl-4-isoxazolepropionic acid; GluA1-4), kainate (GluK1-5) and NMDA (N-methyl-D-aspartate; GluN1, GluN2A-D and GluN3A-B) receptors. Crystallographic and Cryo-EM studies in recent years have provided detailed structural information of these membrane-spanning iGluRs (overview in (Kumar & Mayer 2013; Sobolevsky 2015)). They are tetrameric complexes composed of homologous subunits. Each subunit has a conserved modular design and is composed of an extracellular N-terminus (NTD), an extracellular ligand-binding domain (LBD), an intracellular C-terminus (CTD), three transmembrane domains (M1, M3 and M4) and one pore loop (M2)(Sobolevsky 2015) (**Figure 17 B**). The latter inserts into the membrane from the intracellular side and forms together with the M3 segment the channel pore (Wollmuth & Sobolevsky 2004). The modular architecture of iGluRs suggests that they have descended from a common ancestral prokaryotic receptor. Notably the complex domain architecture of all eukaryotic iGluRs is partially conserved in a simple bacterial iGluR from *Synechocystis* (called GluR0; (Chen et al. 1999)), indicating an origin of all eukaryotic iGluRs before the prokaryote-eukaryote dichotomy occurred. However, although a structural overall similarity between the LBD and the transmembrane domains composed of the segments M1-M3 has been proposed (Janovjak et al. 2011; Chen et al. 1999), the bacterial GluR0 differs significantly from its eukaryotic counterparts and lacks the NTD, M4 and CTD. Interestingly, the LBD and channel pore domain of iGluRs are structurally related to other bacterial proteins, i.e. the substrate

binding proteins (SBP) and potassium (K⁺)-channels, respectively (O'Hara et al. 1993; Wood et al. 1995; Kuner et al. 2003). For both bacterial protein family's crystallization has yielded detailed structures with related function and highlighted the idea that SBPs and K⁺-channels are functional homologous to the LBD and the M1-M3 segment of iGluRs, respectively. Therefore an evolutionary link between these bacterial protein families and the GluR0 was proposed which might arise by the insertion of an inverted K⁺-channel pore between the SBP domains leading to the formation of a modular prototype of potassium-specific channels (i.e. GluR0) (Chen et al. 1999) (see for illustration Fig. 1A). Prokaryotic SBPs facilitate chemotaxis and substrate uptake of a large variety of small molecules and ions by binding their ligands with high specificity and affinity. Interestingly, SBPs share also a common ligand binding mechanism with the LBD of iGluRs consisting of two lobed domains (S1 and S2) connected by a hinge forming a clamshell like structure (O'Hara et al. 1993). Ligand binding takes place at the interface between the two domains, inducing a domain closure. This conformational change functions as the key element in the transition of ligand recognition and ion channel gating in iGluRs (Moore et al. 2013; Mayer et al. 2001). K⁺-channels are selective for potassium ions and comprise a large family of ion channels. All K⁺-channels share the same core topology and tetrameric structure and differ only in the presence or absence of additional transmembrane helices and of additional non-membrane domains. The basic channel-forming core is composed of two transmembrane helices (TM1 and TM2; called S5 and S6 in voltage-dependent Kv channels) with low sequence similarity between the different K⁺-channels. The TM1 and TM2 domains are separated by a pore loop (P-loop), which inserts into the membrane from the extracellular side and contains a conserved 'TXXTVGYG' signature sequence of all K⁺-channel selectivity filters (Heginbotham et al. 1994; Kuang et al. 2015). However, although K⁺-channels and the pore-forming core domain of iGluRs share a common architecture, the K⁺-channel selectivity filter is not conserved and the pore-forming core domain of the K⁺-channel shows an inverted orientation in the membrane. Nevertheless, the apparent sequence and structural similarities of the different domains led to the hypothesis that the GluR0 is a modular composition of an inverted bacterial K⁺-channel and a SBP and represents the precursor of mammalian iGluRs (Wood et al. 1995). A functional compatibility between the pore structure of a K⁺-channel and the LBD of an iGluR could yet not been demonstrated, although several studies tried without success to fuse the LBD of iGluRs with diverse K⁺-channels. Based on these negative results the hypothesis of a compatible architecture of iGluR and K⁺-channel pores was rejected (Hoffmann et al. 2006; Sobolevsky et al. 2003). Here, I revisit the possibility of fusing the membrane-spanning domain of the small viral KcvATCV-1 potassium channel to the glutamate-binding LBD of the AMPA iGluR subunit (GluA1) for creating a functional glutamate-gated potassium channel. It has been shown that small viral K⁺-channels are because of their

structural simplicity, functional robustness and the absence of any coevolution with cellular proteins most suitable as building blocks in synthetic channels where they maintain their conductive properties in the presence of attached regulatory domains (Arrigoni et al. 2013; Di Francesco 2011; Cosentino et al. 2015). With this approach I can show that fusion of the LBD of GluA1 to the minimal K⁺-channel pore of Kcv_{ATCV-1} generates a truly glutamate-gated K⁺-channel. Collectively this provides experimental support for the hypothesis of a phylogenetic link between iGluRs and K⁺-channels. It also implies a conserved activation mechanism of the pore region of iGluRs and ancestral viral K⁺-channels, which is gated by mechanical coupling to the LBD.

4.2. Results

4.2.1. Construction of glutamate-gated $\text{Kcv}_{\text{ATCV-1}}$ chimeras

To investigate a putative functional compatibility of the pore structure of K^+ -channels and mammalian iGluRs, I substituted the channel forming transmembrane domain region of the AMPA GluA1 by a minimal K^+ -channel of viruses named $\text{Kcv}_{\text{ATCV-1}}$ for K^+ -channel from chlorella virus (see for illustration **Figure 17 B**). These viral channel proteins have the structural and functional hallmarks of pro- and eukaryotic K^+ -channels (Thiel et al. 2011), but are composed

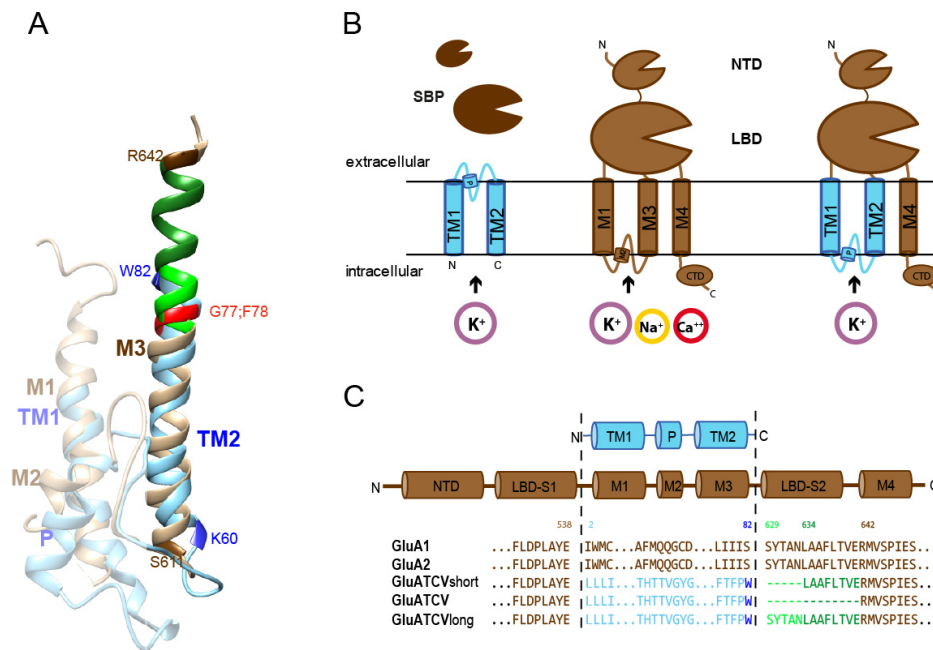


Figure 17 Design of $\text{Kcv}_{\text{ATCV-1}}$ /GluA1 chimeras. (A) Schematic representation of a viral potassium channel, substrate binding proteins and eukaryotic glutamate receptors. Cartoon depicting the topology and domain organization of a subunit of the $\text{Kcv}_{\text{ATCV-1}}$ (blue), GluA1 (brown) and the chimera GluATCV harboring the membrane-spanning domain of the $\text{Kcv}_{\text{ATCV-1}}$. Amino-terminal domain (NTD), ligand-binding domain (LBD), C-terminal domain (CTD), pore helix (P), transmembrane domains (TM respectively M in case of GluA1), substrate-binding-protein (SBP, dark brown). Permeant cations are indicated. (B) Structural overlay of the pore forming domains of $\text{Kcv}_{\text{ATCV-1}}$ and GluA2. The TM1 and the pore helix as well as the M1 and M2 of GluA2 are shown transparent. The transmembrane domain 2 of the $\text{Kcv}_{\text{ATCV-1}}$ (TM2) and the GluA2 (M3) are shown in full color. Helices were superimposed by aligning main-chain atoms of the TM2 segments of a $\text{Kcv}_{\text{ATCV-1}}$ model (**2 Material and Methods**) on the crystal structure of the M3 domain of the GluA2 subunit (Protein Database entry 3KG2; 20) (side view). Backbones with corresponding residues of the subunits are illustrated in ribbon representations (blue: $\text{Kcv}_{\text{ATCV-1}}$; brown: GluA2) with the in iGluRs conserved SYTANLAAF region in green and the position of G77 and F78 of $\text{Kcv}_{\text{ATCV-1}}$ in red. (C) Design of GluATCV constructs. Partial sequence alignment of the GluA1 (Rat), GluA2(Rat) and the different GluATCV constructs. Illustration of the amino acid cutting sites of the different GluA1/ $\text{Kcv}_{\text{ATCV-1}}$ chimeras (GluATCV) used. Chimeras harboring different lengths of the SYTANLAAF motif (green) with the corresponding residue numbering of the mature subunits ($\text{Kcv}_{\text{ATCV-1}}$ blue; GluA1 brown) are indicated. GluATCVlong (linker length +13 aa); GluATCVshort (linker length +8 aa) and GluATCV (no linker). Residues found at the cutting sites and within the SYTANLAAF motif are highlighted. Secondary structure elements found in GluA2 are illustrated above the sequence.

of only 82 amino acids. The combination of structural simplicity and robust function suggest that Kcv-type channels are the minimal unit of a functional K^+ -channel pore module. A structural overlay of a homology model of the Kcv_{ATCV-1} (**2 Material and Methods**) on the crystal structure of the transmembrane domains of the GluA2 subunit (Protein Database entry 3KG2; (Sobolevsky et al. 2009) in combination with published sequence alignments (see(Gazzarrini et al. 2003; Price et al. 2012; Tikhonov & Magazanik 2009)) revealed that the TM2 helix of the Kcv_{ATCV-1} is about eight amino acids shorter than the M3 and TM2 domain of canonical iGluR and K^+ -channels, respectively. Remarkably, the last amino acids of the C-terminal helix of TM2 in Kcv_{ATCV-1} overlap with the N-terminal sequence of the highly conserved SYTANLAAF motif in iGluR linking the M3 to the LBD (**Figure 17 A**; (Chang & Kuo 2008)).

Inspired by this homology I generated an initial AMPA GluA1 receptor chimera (GluATCV_{short}; **Figure 17 C**) by inserting the Kcv_{ATCV-1} pore at position 538 and 634 of the GluA1. In this construct the TM2 helix of the viral protein was extended by the rest of the C-terminal part of the SYTANLAAF motif to match the total M3 length of iGluRs. To avoid glutamate-mediated channel desensitization, I used a construct containing the desensitization attenuated mutant L479Y in the LBD of the GluA1 (Stern-Bach et al. 1998; Kott et al. 2009) in all following experiments.

When I analyzed GluATCV_{short} by two-electrode voltage clamping in *Xenopus laevis* oocytes, I could not elicit any currents in response to 1 mM glutamate (Glu). Remarkably, compared to control oocytes, I observed a large leakage current (I_{leak}) in the range of $0.9 \pm 0.3 \mu A$ in the

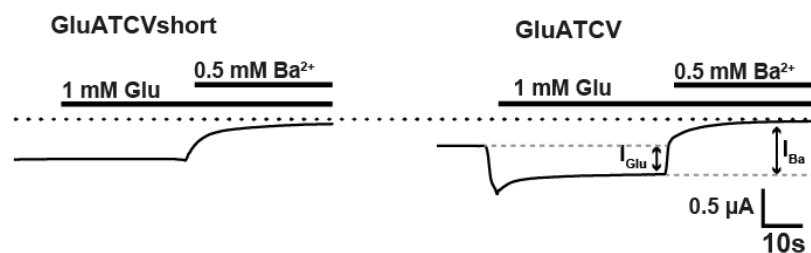


Figure 18 Functional characterization of chimeric GluATCV constructs. Representative whole-cell currents of Glu responses and Ba^{2+} inhibition of GluA1/Kcv_{ATCV-1} chimeras upon heterologous expression in *Xenopus* oocytes recorded at -70 mV membrane potential. Oocytes expressing the GluATCV_{short} and GluATCV were superfused with the indicated concentration of Glu in the absence and presence of 500 μM Ba^{2+} . Current traces illustrating the inhibitory effect of Ba^{2+} in both chimera. Note that the K^+ -specific antagonist Ba^{2+} inhibits both the glutamate-induced currents elicited from GluATCV and the leak current in GluATCV_{short} expressing oocytes. Black dotted line indicates the Ba^{2+} insensitive leakage current. Bars show timepoint and duration of the application. Gray dotted line and arrows indicate the glutamate induced current (I_{Glu}) and the Ba^{2+} blockable current (I_{Ba}).

absence of the agonist which could be efficiently blocked by the specific K⁺-channel blocker Ba²⁺ (93.5 ± 1.6 %; $n = 5$; **Figure 18**; Table 1) (Gazzarrini et al. 2009), but not with the specific competitive Glu antagonist CNQX. From these data I reasoned that the pore domain of the Kcv_{ATCV-1} converted the GluATCV_{short} construct into a K⁺-channel-like behavior, which, however, could not be gated by external Glu. Since the M3-LBD linker is a crucial element in iGluR gating (Moore et al. 2013), I generated two additional constructs with variable lengths of the TM2 helix (**Figure 17 C**). Strikingly, although the new construct with a 13 amino acid deletion including the SYTANLAAF motif (GluATCV; **Figure 17 C**) showed again a high leakage current (0.6 ± 0.2 μ A; Table 1), it responded in a robust manner to Glu. Application of the ligand elicited currents with 0.4 ± 0.3 μ A in amplitude (**Figure 18**; $n = 10$). In contrast, the construct containing the whole SYTANLAAF motif (GluATCV_{long}; **Figure 17 C**) behaved likewise to the initial GluATCV_{short} construct and remained insensitive to Glu application. Both, the initial leakage and the Glu-induced currents of the GluATCV could be blocked by Ba²⁺ (**Figure 18**). Quantitative analysis of the Ba²⁺-sensitive Glu-induced response and the resting leakage current ($I_{\text{Glu}}/I_{\text{Ba}}$) revealed that 36.4 ± 4.6 % ($n = 5$) of the total Ba²⁺-sensitive currents in the GluATCV construct could be specifically induced by Glu-application (**Table 2**). The results of these experiments indicate that the substitution of the pore forming transmembrane domains of the GluA1 by a minimal viral K⁺-channel resulted in a Glu-gated K⁺-channel with a relatively high spontaneous activity in the resting state.

Table 2 Leakage currents and fractional Ba²⁺-sensitivity of control and GluATCV_{short}, GluATCV and GluATCV* expressing oocytes:

	Uninjected	GluATCV _{short}	GluATCV	GluATCV*
Initial leakage current [μ A]	0.1 ± 0.06	0.9 ± 0.3	0.6 ± 0.2	0.2 ± 0.1
Ba ²⁺ -block of the leakage current [%]	<10 %	93.5 ± 1.6	84.4 ± 2.3	$32.9 \pm 10.8^{***}$
Glutamate-induced fraction of the Ba ²⁺ -block [%]	n.d.	n.d.	36.4 ± 4.6	$68.2 \pm 5.2^{**}$

The three constructs differ in the leakage currents and Ba²⁺ sensitivity. Note that the fractional contribution of the Ba²⁺-sensitive leakage current to the overall leakage and of the Glu-induced current to the total Ba²⁺-sensitive current are highly significantly different between GluATCV and GluATCV* expressing oocytes. n.d., not detectable.

4.2.2. Increase of glutamate efficacy

It is known that Kcv_{ATCV-1} has a high intrinsic open probability (P_o) (Thiel et al. 2011), suggesting that the high leakage current of the GluATCV construct might be due to a high intrinsic spontaneous activity of the Kcv_{ATCV-1} pore domain. To test this hypothesis, I exploited a recent finding of the related Kcv_{NTS} channel, where two substitutions had been shown to greatly reduce P_o (Rauh et al. 2017). I therefore analyzed the P_o of the wt Kcv_{ATCV-1} and the corresponding double-mutant Kcv_{ATCV-1}^* by functional reconstitution in planar lipid bilayers.

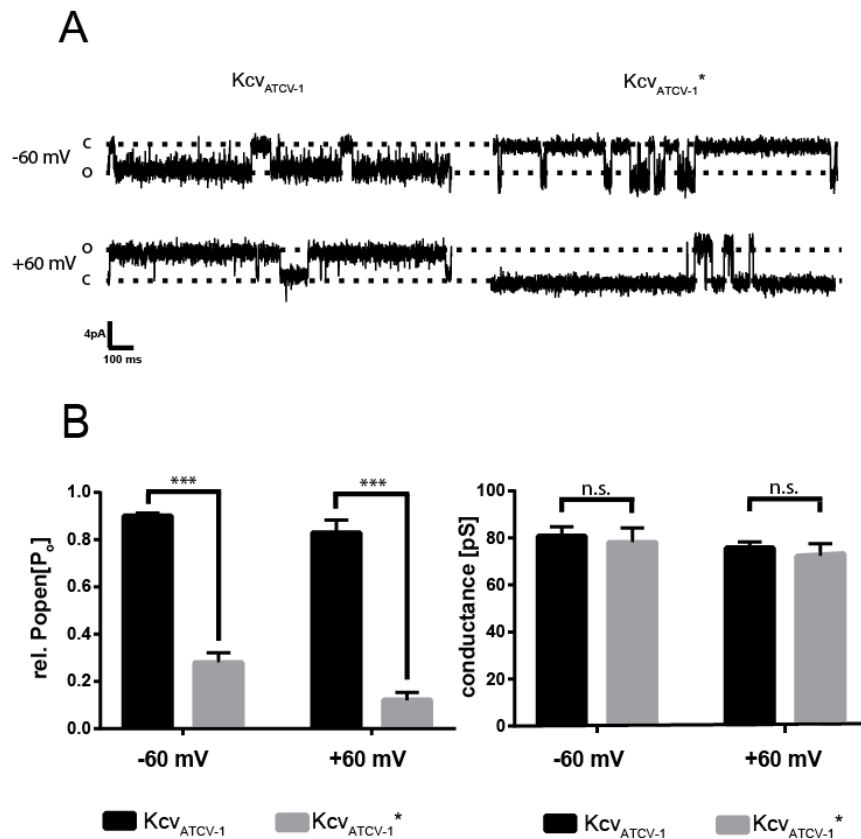


Figure 19: Influence of the open probability of Kcv_{ATCV-1} by TM2 point mutations (A) Single channel recordings of the Kcv_{ATCV-1} and Kcv_{ATCV-1}^* . Currents of Kcv_{ATCV-1} and Kcv_{ATCV-1}^* (mutated at aa positions (G77S, F78L) were recorded at a membrane potential of +60 mV and -60 mV upon reconstitution in planar lipid bilayer (**2 Material and Methods**). Note the difference of the open probability in the characteristic single channel fluctuations of the two K⁺ channels. (B) Analysis of the open probability and single channel conductance of Kcv_{ATCV-1} and Kcv_{ATCV-1}^* . Plot of the open probabilities (P_o) and single channel conductance (pS) of the wt and mutant Kcv_{ATCV-1} channel by calculating the time of occupancy of the open state (O) and the closed state (C) from 4 independent 1 min recordings at +60 and -60 mV ($p < 0.001$; $n = 4$).

Consistent with the data of the related Kcv_{NTS} , substitution of G77 to S and F78 to L caused also in the Kcv_{ATCV-1} a significant reduction in the P_o from 0.83 ± 0.11 to 0.14 ± 0.01 in the Kcv_{ATCV-1}^* mutant at -60 mV (**Figure 19**; $p < 0.001$; $n = 4$) without altering single channel conductance

(79 ± 6.1 pS and 81 ± 4.0 pS for the GluATCV and GluATCV*, respectively; **Figure 19 B**). In the next step I tested whether these mutations alter the ratio $I_{\text{Glu}}/I_{\text{Ba}}$ in the GluATCV construct.

The results in **Figure 20 A** show that the double mutant G614S/F615L in the GluATCV* (* for low intrinsic spontaneous activity) generates indeed the expected effect. GluATCV* generated currents with a drastic reduced leakage component ($I_{\text{leak}} = 0.2 \mu\text{A} \pm 0.1$; $n = 5$) and a concomitant increase in the amplitude of the Glu-inducible current (**Figure 20**; $I_{\text{Glu}} = 0.7 \pm 0.2 \mu\text{A}$; $n = 5$).

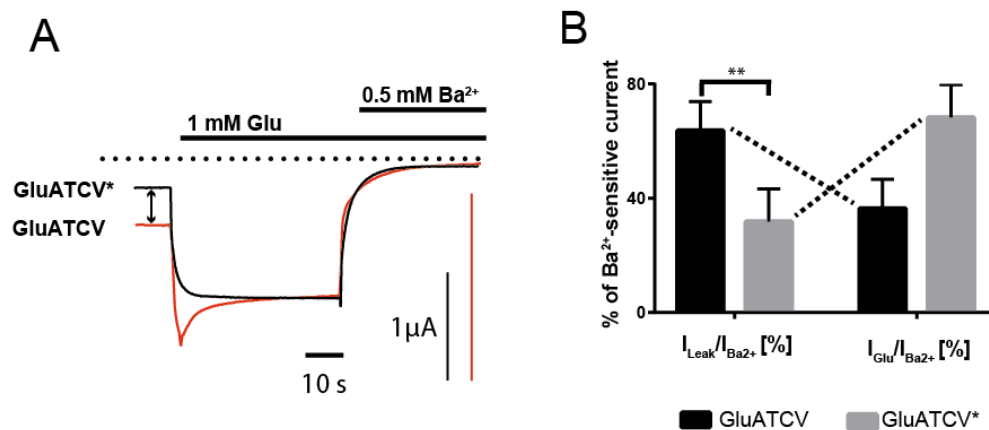


Figure 20 Increase of Glu-gating efficiency in GluATCV by TM2 point mutations (A) Overlay of representative recordings of glutamate (Glu) responses and Ba^{2+} inhibition at GluATCV (red) and GluATCV* (black). Arrow illustrates the differences in the ratio of the inhibition of the glutamate-induced currents and the resting leakage by the K^{+} -specific antagonist Ba^{2+} in GluATCV and GluATCV* expressing oocytes. Dotted line indicates the Ba^{2+} insensitive leakage current. (B) Fractional contribution of the Ba^{2+} -sensitive leakage- and of Glu-induced currents in GluATCV constructs. Percentage of the Glu-induced currents of the total Ba^{2+} -sensitive current in GluATCV* is highly significant increased compared to the GluATCV (68.2 ± 5.2 % vs. 36.4 ± 4.6 %, respectively; $p < 0.002$; $n = 5$).

Again, both, the glutamate-induced and the leakage currents could be efficiently blocked by Ba^{2+} (**Figure 20 A**) underscoring that both currents are generated by the GluATCV* channel. The reduced spontaneous activity of the pore domain in the GluATCV* construct, the contribution of the Glu-induced current to the total current increased by a factor of 2 (GluATCV* 68.2 ± 5.2 % vs. GluATCV 36.4 ± 4.6 %; **Figure 20 A Table 2**; $p < 0.002$; $n = 5$) by the 2-fold decrease in the Ba^{2+} -sensitive leakage currents (**Figure 20 B**). Remarkably, although the fractional contribution of the Ba^{2+} -sensitive leakage and Glu-induced currents were inversely affected in the GluATCV and the GluATCV* constructs, the maximal Ba^{2+} -sensitive currents were not different (GluATCV $1.0 \pm 0.3 \mu\text{A}$ vs. GluATCV* $0.8 \pm 0.2 \mu\text{A}$). The results of these experiments suggest that the overall expression and activity of the two

constructs were similar and that a high intrinsic spontaneous activity of the channel pore hampers the efficiency of the Glu-induced channel opening in the GluATCV constructs.

4.2.3. Pharmacological characterization of the GluATCV*

For a first pharmacological characterization of the GluATCV*, I determined dose-response curves for Glu and calculated the respective EC_{50} values for the parental GluA1 and GluATCV*. Remarkably, neither the resulting Glu-induced current traces nor the EC_{50} values of the GluATCV* were distinguishable from those of the GluA1 receptor (Figure 21 A, B). Both showed desensitization attenuated Glu-currents with similar EC_{50} values ($5.8 \pm 1.2 \mu\text{M}$ and $4.0 \pm 0.4 \mu\text{M}$ for the GluATCV* and GluA1, respectively; $p = 0.2$; $n = 8$). Similarly, inhibition curves with the competitive AMPA antagonist CNQX revealed an IC_{50} value comparable to *wt* GluA1 ($4.4 \pm 0.9 \mu\text{M}$ and $2.0 \pm 0.1 \mu\text{M}$ for the GluATCV* and GluA1, respectively; $p > 0.05$; $n = 5$; Figure 21 C). These data show that insertion of a Kcv_{ATCV-1}^* channel pore did neither

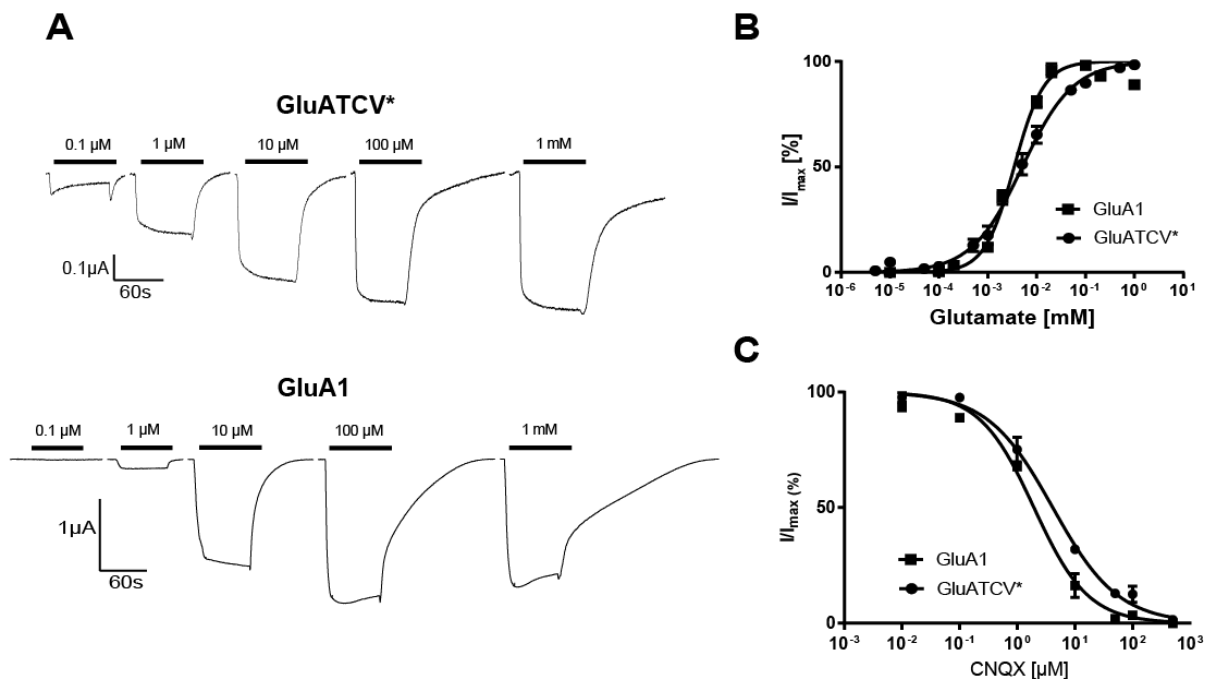


Figure 21 Functional characterization of the GluATCV chimera. (A) Glu responses of GluA1 and GluATCV* upon expression in *Xenopus* oocytes. Traces of Glu responses of GluA1 and GluATCV* with different concentration of Glu. The bars show the duration of the application of the corresponding concentration. (B) Glu-dose response curves recorded from GluA1 (squares) or GluATCV* (circles) expressing oocytes. Both show a similar EC_{50} value of $5.8 \pm 1.2 \mu\text{M}$ and $4.0 \pm 0.4 \mu\text{M}$ for GluATCV* and GluA1, respectively. (C) CNQX-inhibition curve of GluA1 and GluATCV* at the EC_{50} value of Glu. The CNQX IC_{50} is $4.4 \pm 0.9 \mu\text{M}$ and $2.0 \pm 0.1 \mu\text{M}$ for GluATCV* and GluA1, respectively.

affect i) the amplitude of the current responses nor ii) the apparent agonist and antagonist-affinity.

In summary, these results show that the GluATCV* pharmacology is comparable to the pharmacology of the native GluA1 channel.

In further experiments I examined the ion selectivity of GluATCV*. Since the GluA1 channel exhibits no selectivity for K^+ over Na^+ (Ferrer-Montiel et al. 1996), I tested whether insertion of the Kcv_{ATCV-1}^* channel converts the unspecific GluA1 monovalent cation channel into a specific K^+ -selective channel by ion substitution. Analysis of Glu-induced current/voltage (I/V)-curves in bath solutions in which K^+ was replaced by Na^+ showed that the GluATCV* caused, different to GluA1, a shift of the reversal voltage as a function of the extracellular K^+ concentration: the shift in reversal voltage of GluATCV* can be fitted with a Nernst equation

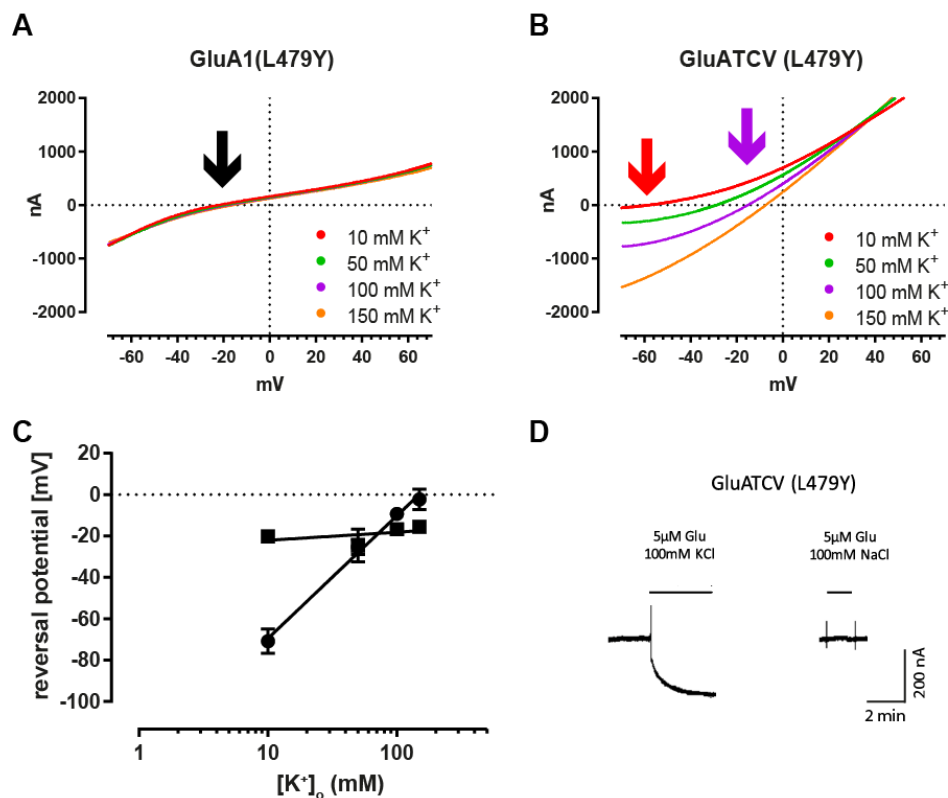


Figure 22 Potassium selectivity of GluATCV*(A) GluA1 ramps with different concentrations of potassium. The ionic strength was normalized by sodium. All curves show a similar reversal potential. (B) Voltage ramp at GluATCV with different potassium concentrations. A right shift of the reversal potential with increasing potassium concentration. (C) Plot of the reversal voltages of the GluA1 and GluATCV* receptors against the extracellular K^+ concentration. Reversal voltages were estimated by current-voltage (I-V) recordings in different ringer solutions containing 10, 50, 100 or 150 mM K^+ . The proportional shift of the reversal voltage as a function of the concentration of K^+ in the extracellular medium with a slope of 59.3 ± 4.9 for the GluATCV* and 3.9 ± 4.7 for GluA1 confirms a high selectivity for K^+ over Na^+ in the GluATCV* channel. (D) Application of glutamate at the same GluATCV expressing oocyte with 100 mM K^+ or 100 mM Na^+ solution show that only in presence of potassium the receptor opens.

providing a mean shift of 59.3 ± 4.9 for a 10-fold increase in $[K^+]_o$. In the same experiments GluA1 only responds with a shift of 3.9 ± 4.7 to a 10-fold change in $[K^+]_o$ (**Figure 22**). This shift in the reversal voltage confirms a high selectivity for K^+ over Na^+ in the GluATCV* channel. The $P(Na^+)/P(K^+)$ ratio can be calculated by the Goldman-Hodgkin-Katz equation under bi-ionic conditions and is with 0.04 ± 0.01 similar to that of Kcv_{ATCV-1} (Gazzarrini et al. 2009), but significantly different from that of the nonselective GluA1 channel ($P(Na^+)/P(K^+)$ of 0.87 ± 0.02 ; $p < 0.05$; see also (Egebjerg & Heinemann 1993; White et al. 2016)). Collectively my results show that the GluATCV* chimera functions as a K^+ -selective, glutamate-gated channel. It combines both, the characteristics of ligand recognition of the GluA1 iGluR and the selectivity of the Kcv_{ATCV-1} .

4.3. Discussion

In this chapter I construct a chimera out of the mammalian GluA1 and the viral KcV_{ATCV-1} to investigate the possible relation between potassium channel and glutamate receptors. By the functional characterization of this chimera my data demonstrate that a naive coupling of the ligand binding domain (LBD) of the mammalian GluA1 subunit from the ionotropic glutamate receptor family (iGluR) with the viral potassium channel KcV_{ATCV-1} generates a K⁺-selective, Glu-gated receptor channel. This functional compatibility of the LBD of an iGluR with the minimal pore domain of a K⁺-channel underscores a modular architecture with a conserved activation mechanism within the two families and highlights their phylogenetic link. A functional coupling of the two orthogonal domains also provides a tool to understand the most basic mechanical interactions between ligand recognition and channel gating irrespective of co-evolutionary constraints. Ultimately it may foster the design of new K⁺-selective biosensors for specific analyte recognition.

For many years it has been suggested that the pore modules of K⁺-channels and iGluRs share a similar architecture and that they might have a common evolutionary ancestor (Wood et al. 1995; Kuner et al. 2003). This idea of a direct phylogenetic link has been supported by similarities in amino-acid sequences and homologies in structural details of the respective pore domains (Kuang et al. 2015; Bavro et al. 2012; Uysal et al. 2009; Sobolevsky et al. 2010; Karakas & Furukawa 2014). However, an experimental affirmation of this hypothesis by demonstrating a functional convertibility of an iGluR and a K⁺-channel was not provided so far. In contrast, data from several studies argue against a compatible architecture of iGluR and K⁺-pores (Hoffmann et al. 2006; Sobolevsky et al. 2003). Here I can show that a chimeric construct between the LBD of the mammalian GluA1 and the viral potassium channel KcV_{ATCV-1} functions efficiently as a K⁺-selective (**Figure 22**), glutamate-gated ion channel (**Figure 21**) with the specific characteristics of ligand recognition of the iGluR and the ion selectivity of the K⁺-channel. This result strongly supports the idea of a modular design of iGluRs in which the pore originated from an ancestral K⁺-channel (**Figure 17**). Furthermore, the results shed some light on a common molecular mechanism for the activation of P-loop channels in general. In particular, my initial rationale to use a minimal viral K⁺-channel for linking an iGluR LBD was, that the helical segment of the inner TM2 in KcV_{ATCV-1} is too short to interfere with the endogenous iGluR channel gate (SYTANLAAF-motif gate; overview in (Schmid et al. 2007; Sobolevsky et al. 2010; Moore et al. 2013)). Therefore, I assumed that including the SYTANLAAF motif of the iGluR of my constructs might render the viral K⁺ channel sensitive to

LBD-mediated gating. I found however that this motif is not essential for Glu-induced K⁺-channel gating; it can be substituted by an endogenous, so far not anticipated K⁺-viral gate. Glut-gated channel opening is thought to be mediated via an iris-like conformational change in the TMs (Twomey et al. 2017) by pulling the M3 pore-forming helices away from the central pore axis upon Glu-binding (Sobolevsky et al. 2009; Kumar & Mayer 2013; Stephen F Traynelis et al. 2010; Wollmuth & Sobolevsky 2004). This proposed mechanism is comparable with K⁺-channel gating (Doyle 2004; Jiang et al. 2002). This simple mechanical model, which is supported by molecular dynamics simulations and combined functional and computational studies (Dai et al. 2015; Kazi et al. 2014), predicts that the closed-to-open free energy of the channel should be related to the tension within the LBD-M3 linker; the channel open probability should be determined by the LBD-M3 linker length. However, based on recent cryo-EM studies in the GluA2 (Twomey et al. 2017) this view of a simple action of the linkers as a rigid mechanical lever has been challenged. Here, based on the 2-fold symmetrical arrangement of the LBDs, the S2-M3 linkers connecting the LBDs to the pseudo-4-fold symmetrical channel form two conformational distinct diagonal pairs and contribute geometrically and energetically different to channel opening (Twomey et al. 2017). The differential contribution of the linker pairs result in an inherent asymmetric state of the M3 helices, which is similar to a recently described pairwise asymmetric “dimer of dimers” state proposed by a kink in the inner TM2 domain in viral potassium channels (Rauh et al. 2017). Thus, although the gating hinges in the TM2 of potassium channels and in the M3 of iGluRs seem to be different and structurally unique, I think that the 2-fold changes in the M3 of iGluRs mediated by LBD dimers and the pairwise asymmetric state in the TM2 during viral K⁺-channel gating are converted to channel opening; this mechanism seems to be conserved in tetrameric P-loop ion channels. This may sufficiently explain the functionality of my minimal construct by a phylogenetically conserved, pairwise adopted asymmetric channel configuration during channel opening below the principal rotational symmetry of the pore.

Finally, my results are consistent with a modular architecture of iGluRs and a phylogenetic link between these proteins and K⁺-channels. Chiu and colleagues (Chiu et al. 1999) proposed that the core function of iGluRs occurred before animals and plants separated from a common albeit unknown prokaryotic ancestor. The present data support the view that a key stage in the evolution of iGluRs was presumably the insertion of an inverted potassium channel pore domain between the two parts (S1 and S2) of a bacterial substrate binding protein (SBP). Despite a low sequence identity, SBPs are structurally homologous to the LBD of iGluRs and share a common ligand binding mechanism. Thus, it can be assumed that the fusion of the two proteins may have occurred in prokaryotes. This is reflected in the K⁺-selective GluR0 channel lacking the

NTD and M4 domains. Indeed, homology modelling and simulation studies of GluR0 supports a degree of common fold and functional similarity between the pore-forming region in GluR0 and the prokaryotic K⁺-channel KcsA (Arinaminpathy et al. 2003). In this study, I report the functional characterization of GluATCV, where a eukaryotic iGluR LBD was successfully functionally linked to a K⁺-channel pore. Interestingly this was achieved by using a viral potassium channel, e.g. a channel which is from a structural point of view very simple and evolutionary ancient (Thiel et al. 2013). Collectively these data support the idea of an ancient phylogenetic link between iGluRs and K⁺-channels. The present data furthermore underscore that a primitive channel with poor control on gating can acquire sophisticated ligand mediated regulation via a naive coupling with an orthogonal ligand binding domain. This prove of concept finding makes it supposable that ligand gated channels occurred as a result of a singular evolutionary step. Following this line of thought I also predict that synthetic GluATCV channels can now offer an excellent experimental system for understanding structure/function correlates in complex glutamate receptors. In a learning-by-building approach the synthetic channels can now be engineered in such a way that they exhibit the functional behavior of complex glutamate receptors. In this way it will be possible to understand in an unbiased manner the basic structural interactions between the sensing and the pore unit, which are crucial for the function of complex GluR.

5. Project III - Reduction of the chimera on the core parts of a receptor

Chapter III is published in the same or similar form as Schönrock et al. 2019 in communications biology.

5.1. Introduction

Eukaryotic glutamate receptors no matter if they are NMDA, AMPA or Kainat receptors all share the same construction. They consist of two TM (M1, M3) pore forming domains looking like an inverted potassium channel and a third TM the M4 in the membrane spanning region. Extracellularly they all consist of a clamshell like ligand binding domain. This LBD ether binds glutamate (AMPA, Kainat, NMDA receptors) or glycin (NMDAR) and leads by a closure of the clamshell to a structural change transducing the forces build up while the closing to the transmembrane domain and opening the pore (Stephen F. Traynelis et al. 2010; Twomey et al. 2017). This structural reorganization allows an ion flux trough the pore. Connected to the LBD a second clam shell looking structure is associated. This structure called the amino terminal domain (NTD) is a binding region for some modulators and was former supposed as necessary for receptors assembly (Ayalon et al. 2001). This idea was rejected with functional measurements of truncated receptor versions without NTD. In 1998 the discovery of the GluR0 a bacterial version of glutamate receptors throws a new light on necessary domains for receptors. The GluR0 also consists out of a two TM channel pore but without a third TM. Also, in the extracellular region no NTD is existing. In the GluR0 the NTD and the M4 are totally non-essential for a functional receptor (Chen et al. 1999) while the deletion of the M4 in eukaryotic glutamate receptors leads to an unfunctional receptor (Salussolia et al. 2011). Out of experiments with M4 truncated NDMAR it is known that the coexpression of the detached TMD is sufficient to recover the receptor function (Schorge & Colquhoun 2003). In AMPA receptors the M4 is associated with the oligomerization and surface expression (Salussolia et al. 2011; Salussolia et al. 2013).

To illuminate the tasks of both the NTD and the TMD more precise I used my previous designed glutamate gated potassium channel (see chapter 4) in truncated versions and investigated the functionality via TEVC.

5.2. Results

5.2.1. Design of a minimal glutamate-gated potassium channel

To investigate the minimal structural requirements for a functional Glu-gated Kcv channel I successively truncated GluA1 domains from the GluATCV* (see chapter 4). Therefore I designed three constructs. One without the NTD (GluATCV* Δ NTD), a second with an additional deletion of the M4 (GluATCV* Δ NTD Δ M4) and a third one with cysteine modification (GluATCV* Δ NTD Δ M4 V152/N402C) (compare **Figure 23** left). First, I examined whether an N-terminally truncated GluATCV* construct that lacks amino acids 19 to 395 of the mature subunit (GluATCV* Δ NTD,

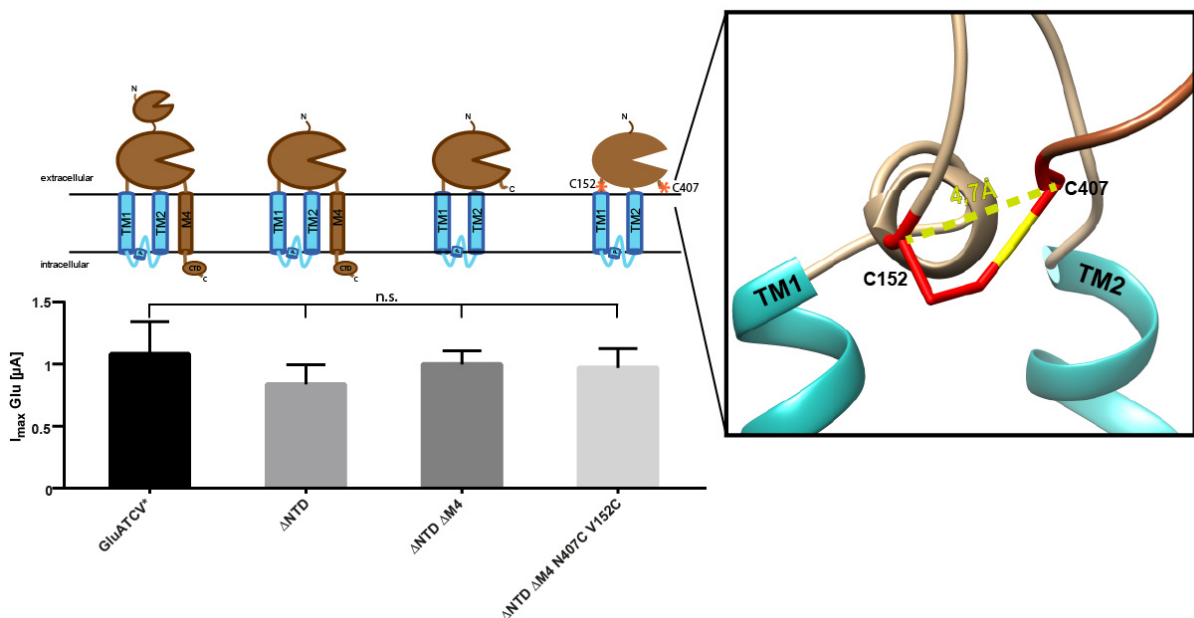


Figure 23 Schematic drawings and functional expression of the deletion and mutant constructs used. Cartoons depicting the NTD- and the M4 truncated versions and the cysteines mutated (indicated by red stars); Inset: Point mutations in the LBD (N407C) and TM1 segment (V152C) thought to form a disulfide-bridge are highlighted in red based on my homology model against 3KG2. Numbers correspond to amino acid positions in the mature protein. I_{max} currents of each mutant, with and without DTT in the case of the cysteine double mutant, are shown ($p > 0.05$; $n = 4-10$).

Figure 23) forms functional receptors in *X. laevis* oocytes. **Figure 23** shows that receptors composed of the NTD-deleted GluATCV* Δ NTD subunit still displayed robust agonist responses. In the presence of saturating glutamate concentrations, the I_{max} values were similar to those of the full-length GluATCV* receptor (**Figure 23**; $I_{max} = 1.0 \pm 0.26 \mu$ A; $p = 0.8$; $n = 5$), indicating that the N-terminal domain is neither essential for GluATCV assembly nor for function. Next, a C-terminal truncated GluATCV* Δ NTD subunit was generated by deleting residues downstream of

V784 including transmembrane domain M4 and the whole C-terminal domain (GluATCV* Δ NTD Δ M4; **Figure 23**).

Although 55 % of the initial GluATCV construct is deleted in the GluATCV* Δ NTD Δ M4, I observed desensitization-attenuated currents with similar I_{\max} values after applying Glu at saturating concentrations (**Figure 23**). Since these currents are comparable to those generated by the GluA1 and the full-length GluATCV* receptors (**Figure 24 A**), I reasoned that neither the NTD nor the C-terminal domain (including M4) of the GluA1 in the GluATCV* construct is required for receptor assembly, membrane insertion and functional expression. This prompted me to determine the apparent glutamate affinities of the truncated constructs.

The analysis shows that the Glu-affinities of GluATCV* and GluATCV* Δ NTD Δ M4 receptors were 3-fold different with EC_{50} values of $5.8 \pm 1.2 \mu\text{M}$ versus $20.8 \pm 2.6 \mu\text{M}$, respectively ($p < 0.0001$; $n = 4$; **Figure 24 B**). The affinity in the GluATCV* Δ NTD receptor on the other hand was similar to that of the full-length channel ($5.8 \pm 1.0 \mu\text{M}$). Based on current models of iGluR activation and these data I assumed, that anchoring the LBD to the M4 may be essential for high-affinity

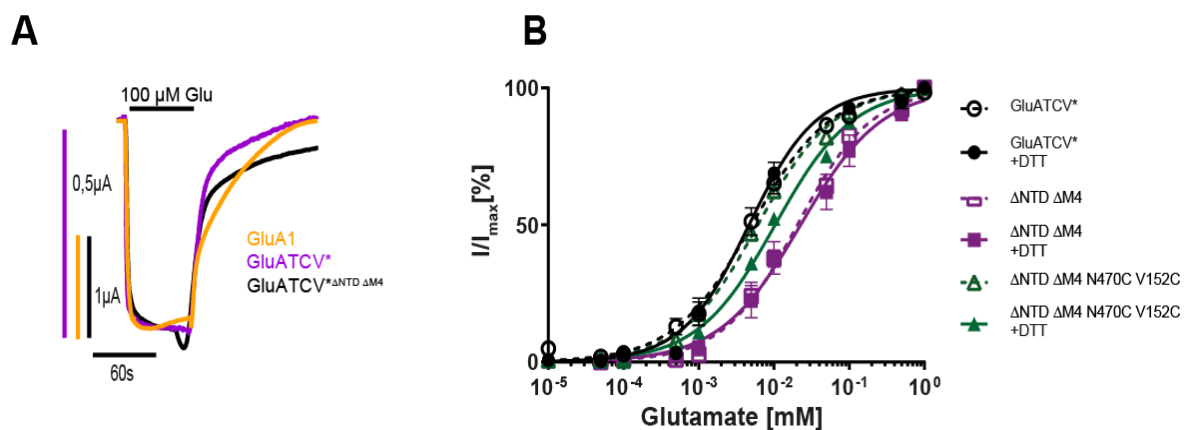


Figure 24 Functionality of the used mutants. (A) Overlay of representative whole cell current traces of Glu-gated GluATCV*, GluATCV* Δ NTD Δ M4 and GluA1. The respective traces in response to application of 100 μM glutamate (Glu) are shown in magenta, black, and orange, respectively. Note that the overall shape of the glutamate-induced whole cell currents is similar between the constructs. (B) Glu dose response curves of GluATCV* (black circles), the deletion mutant GluATCV* Δ NTD Δ M4 (magenta squares), and the double mutant GluATCV* Δ NTD Δ M4 V152/N402C (green triangles) without DTT (open symbols) and in the presence of 5 mM DTT (closed symbols). EC_{50} GluATCV* $5.8 \pm 1.1 \mu\text{M}$ (-DTT) and $5.1 \pm 1.1 \mu\text{M}$ (+DTT); GluATCV* Δ NTD Δ M4 $20.8 \pm 2.6 \mu\text{M}$ (-DTT) and $22.6 \pm 2.9 \mu\text{M}$ (+DTT); GluATCV* Δ NTD Δ M4 V152/N402C $5.9 \pm 0.4 \mu\text{M}$ (-DTT) and $10.5 \pm 0.7 \mu\text{M}$ (+DTT). Note that, in contrast to GluATCV* and GluATCV* Δ NTD Δ M4, only the GluATCV* Δ NTD Δ M4 V152/N402C shows a significantly changed EC_{50} value in the presence of DTT (green closed triangles) indicative of an intrasubunit disulfide link between LBD and TM1.

Glu-binding to GluATCV receptors. To test the importance of LBD-TM interactions for receptor stabilization, I identified in the GluA2 (PDB entry 3KG2) based GluATCV homology model (MatMet) two amino acids in the N-terminal part of TM1 (V152) and at the very C-terminus of the LBD (N407) (**Figure 23** inset). The side chains of these amino acids are directed into the center of the subunit towards an intra-subunit cavity. I measured that the C α atoms are separated by less than 5 Å. This implies that a disulfide bond between the LBD and the TMs could be formed for stabilizing LBD-TM interactions. To test this hypothesis the two residues were substituted by cysteine. The resulting GluATCV* Δ NTD Δ M4 V152C/N407C construct and the GluATCV* and GluATCV* Δ NTD Δ M4 receptors were expressed in oocytes and the Glu-current response recorded in the absence and presence of dithiothreitol (DTT), which reduces disulfide bonds between cysteine residues (Iglesias et al. 2017). The resulting Glu-dose-response curves in the absence of DTT were indistinguishable from those of the M4 containing GluATCV* receptors (GluATCV* and GluATCV* Δ NTD) (**Figure 24 B**). Remarkably, after DTT treatment, only the EC₅₀ value of the GluATCV* Δ NTD Δ M4 V152C/N407C receptor showed a significant 2-fold decrease in apparent Glu-affinity (from $5.9 \pm 0.4 \mu\text{M}$ to $10.5 \pm 0.7 \mu\text{M}$; $p = 0.0004$, $n = 6$) whereas the EC₅₀ values of the GluATCV* and the GluATCV* Δ NTD Δ M4 receptors were not affected by DTT (**Figure 24 B**). At the same time the maximal inducible currents of all constructs tested were not significantly changed by addition of DTT. These data are consistent with the idea that the pair of cysteines, which were introduced in GluATCV* Δ NTD Δ M4 V152C/N407C receptors, are able to form a disulfide bond. Breaking of this bond by DTT resulted in a decrease in apparent Glu-affinity (**Figure 24** and **Table 3**). The results of these measurements suggest that stabilizing of LBD-TM interactions via a linker (exemplified at position 152 and 407) contributes to ligand affinity of GluATCV receptors, in an otherwise complete functional state of the receptor.

Table 3 Overview of EC₅₀ values for different GluATCV* constructs with and without DTT:

	-DTT	+DTT
GluATCV*	$5.8 \pm 1.1 \mu\text{M}$	$5.1 \pm 1.1 \mu\text{M}$
GluATCV* Δ NTD	$5.1 \pm 0.4 \mu\text{M}$	$4.7 \pm 0.4 \mu\text{M}$
GluATCV* Δ NTD Δ M4	$20.8 \pm 2.6 \mu\text{M}$	$22.6 \pm 2.9 \mu\text{M}$
GluATCV* Δ NTD Δ M4 V152C/N407C	$5.9 \pm 0.4 \mu\text{M}$	$10.5 \pm 0.7 \mu\text{M}$

5.3. Discussion

In this chapter I used the functional chimera GluATCV* to investigate the minimal needed parts of a GluR and simultaneously to proof the necessity of the M4 in this chimera. The present data provide implications for the understanding of iGluR assembly. For several years it was thought that the tetrameric assembly of iGluRs are mediated by inter-subunit interfaces including the NTD, LBD and the TMD segments (overview in (Sobolevsky 2015)). This simple view has been questioned by experimental data. By using deletion constructs it has been shown that the NTDs do not play the important role in iGluR assembly (Salussolia et al. 2013; Salussolia et al. 2011) which was previously anticipated. The deletion of this part did not influence the chimera in any way and refute like the other previous studies a crucial function of the NTD in the assembly of GluR. However, the importance of the transmembrane domains in oligomerization remains still controversial. As an additional player, interactions of the TMs with the M4 segment have been implicated as important for subunit assembly (Madry et al. 2007; Mesic et al. 2016; Salussolia et al. 2011; Salussolia et al. 2013; Gan et al. 2015; Amin et al. 2017). To investigate the necessity of M4 in this chimeric receptor I truncated the M4 in addition to the NTD. The present data show that constructs, in which the M4 was deleted, are still able to assemble into functional glutamate-gated channels (**Figure 23**). This argues against a critical role of the M4 for proper receptor assembly. This finding is consistent with data obtained for the NMDAR (Madry et al. 2007; Mesic et al. 2016; Schorge & Colquhoun 2003), where deletion of the M4 domain did not affect receptor assembly and surface expression. Together, these findings are also in line with the functional subunit structure of a bacterial iGluR (i.e. GluR0 from *Synechocystis*), which contains only two TM segments (M1 and M3) and no NTD.

It is worth mentioning that a construct, in which the M4 domain was deleted, displayed a decreased apparent glutamate affinity. This indicates a role of the S2-M4 linker or of the M4 domain in transducing agonist efficacy to channel opening. Changes in the LBD layer are transmitted to ion channel opening by means of the LBD–TM linkers. Although the most important changes seem to occur in the M3–S2 linkers, it has been shown in the GluA2 structure that changes are also observed in S2–M4 linkers (Twomey et al. 2017). This is consistent with either a contribution of the S2–M4 linkers and/or the M4 segment in gating kinetics or a simple stabilization of the LBD via a rigid TM anchor. Using a homology model of the truncated GluATCV* allowed to localize amino acids with distances smaller than 5 Å between the truncated M4 and the TM region. Cysteines with a distance smaller than 5 Å in an aqueous environment could form disulfide bonds (Waschutz et al. 1996) and would allow to imitate the M4 anchor by a bond between this regions. The most promising AA were N407 and V152 (C407 and V152 in **Figure 23** inset). When I used the chimera with introduced cysteines

at the corresponding positions, I find that breaking and forming of a disulfide bond between two cysteines of the C-Terminus of S2 and the TMs affected the apparent glutamate affinity. This indicated that anchoring of the LBDs to the membrane by the M4 may affect M3-S2 linker tension. In an indirect manner the M4 anchor seems to lead by the fixing of the LBD to an enhanced force transduction into the linker TM region and therefor to an earlier or stronger pore opening. This would show one special task of the M4 but should not just the only one.

6. Conclusion

Since several years an interrelation between mammalian glutamate receptors and potassium channels was established, because of a structural analogy between the pore regions which looked similar even though in opposite orientations and the strong sequence homology of glutamate receptors to potassium channels (Wood et al. 1995). Also the resemblance of the ligand binding domain to bacterial binding proteins was assumed as possible evolutionary interaction (Kuner et al. 2003). Although for a long time a direct combination of glutamate receptors and potassium channel as well as pore modification of glutamate receptors were unsuccessful in combination of both protein families. In 1999 a new bacterial GluR (GluR0) gave new ideas of the evolutionary link between the both protein families. The GluR0 showed differently to mammalian GluRs a stronger similarity to potassium channels. It is more selective for potassium than the mammalian GluRs and it also functions without the third transmembrane domain found in mammalian GluR (Chen et al. 1999). With the pore of this bacterial GluR0 the pore of a mammalian GluR could be functionally exchanged for the first time (Hoffmann et al. 2006). Even if this pore chimera was weak potassium selective, it was only a change of domains within the GluR family as the GluR0 is already a glutamate gated receptor. It could not show a true combination of GluR and a pure potassium channel. To investigate the combination of GluR with a pure potassium channel I decided to use a rudimental one, the viral potassium channel Kcv_{ATCV-1}. This channel has the advantage that it is really small, simple and has just the necessary components of a functional potassium channel (Thiel et al. 2011). Within the evolution it seems to be not evolved in coevolution to other proteins and therefore provides a perfect minimal model for potassium channel research. In the first part of my work I considered the orientation of this channel within the membrane as the GluR shows an inverted orientation than the potassium channel. Therefore I used different signal peptides to determine the orientation in HEK293 cells. To investigate the orientation, I used electrophysiological methods and parallel to that immunostainings. Surprisingly my electrophysiological approach indicates, that this Kcv_{ATCV-1} channel at least in HEK293 cells showed an inverted orientation in approximately 30 % of the protein population. To confirm this unusual result, potassium channels are normally orientated in just one direction, I used antibody staining under non permeabilized conditions. Also, these stainings indicated that the Kcv_{ATCV-1} is orientated in again approximately 30 % of the channel population in this unusual direction. This indicated that the use of signal peptides allowed me to determine the direction in an artificial way and showed that the Kcv is functional in both orientations. These first findings led me to the hypothesis, that this channel could also be functional in the inverted part of a GluR. To verify this hypothesis, I designed a chimera of this minimal potassium channel

and a GluR, the GluA1. For the construction of this chimera out of GluA1 and Kcv_{ATCV-1} I built three variants with differences in the length of the M3 LDB linker within the highly conserved SYTANLAAF-motif. In this region a gate of the GluA1 is supposed to be in exactly this SYTANLAAF-motif (Chang & Kuo 2008; Twomey et al. 2017; Sobolevsky et al. 2010). To investigate these different constructs, I used with the TEVC an electrophysiological approach for a functional characterization. Using the different lengths of the STANLAAF-motif to delete this motif completely or stepwise led only to a functional receptor when the whole motif is deleted. In the other cases a pore seems to be built which is blockable like the Kcv_{ATCV-1} by barium but without any Glu-inducible current. Interestingly only the chimera with the complete deleted SYTANLAAF- motif shows, despite the deleted GluA1 gate, a glutamate dependence. This gate within the SYTANLAAF-motif seems to be exchanged by a Kcv_{ATCV-1} intrinsic one which could be also addressed by the GluA1 gating machinery. Additionally, out of these results I concluded, that the linker length seems to be essential for the gating of the pore by the LBD. In this first chimera I recognized in contrast to the GluA1 a high leakage current. This leakage current could occur because of the high open probability of approximately 90 % which is known from Kcv_{ATCV-1}. To enhance the ratio between leakage and glutamate induced current I introduced a mutation which aims a gate in the TM2 of Kcv_{ATCV-1} (Rauh et al. 2017). This mutation reduced the open probability in Kcv_{ATCV-1} from up to 90 % to less than 20 %. The introduction of this mutations in the GluATCV (GluATCV*) reduced the leakage current from 60 % to 30 % and enhanced the glutamate inducible current from 35 % to 70 % at once. Further investigation of the functional chimera in comparison to the GluA1 showed no change in important pharmacological parameters like EC_{50} or IC_{50} . Both are the same with $5.8 \pm 1.2 \mu\text{M}$ against $4.0 \pm 0.4 \mu\text{M}$ in the EC_{50} and $4.4 \pm 0.9 \mu\text{M}$ to $2.0 \pm 0.1 \mu\text{M}$ in the IC_{50} for GluATCV* and GluA1, respectively. The same pore opening mechanism of GluA1 which pulls the M3 out of the pore to open it seemingly allows to open the new Kcv_{ATCV-1} pore. The gate located at the end of TM2 helix of Kcv_{ATCV-1} (Rauh et al. 2017), which I used for enhancing the leakage-glutamate-current ratio, may also be opened by the same mechanism as the GluA1 gate. The selectivity of Kcv_{ATCV-1} for potassium was still present in the chimera. Calculating the relative potassium selectivity over sodium under bi-ionic conditions is with 0.04 ± 0.01 close to the selectivity of the Kcv_{ATCV-1} wildtype (Gazzarrini et al. 2009) while this chimera was still blocked by barium. This shows that the main pore-properties of Kcv_{ATCV-1} are still existing in the chimera. In the third part of my work, I investigated the necessity of the M4 in the designed chimera. As all mammalian GluRs are unfunctional with a deleted M4 and only the bacterial GluR0 was functional without this TM4, I tried to truncate this crucial domain in the chimera. While another minimalization, the deletion of the NTD, does not influence the chimera in any way, the deletion of the M4 led to a shift in the EC_{50} . This brings up the idea that one reason for the

presence of the M4 is the modification of the apparent glutamate affinity by anchoring the LBD to the membrane. To imitate this anchor, I introduced a disulfide bond between the LBD-M4 and the M3-LBD linker to enhance the force distribution. Using this mutant showed a backflip of the E_{c50} to the chimera with a M4. Breaking the disulfide bond, by DTT, allowed a shift in the direction back to the chimera without the M4. The E_{c50} of the GluR0 was with $34 \mu\text{M}$ glutamate similarly to the E_{c50} without the M4, $20,8 \pm 2,6 \mu\text{M}$, in contrast to the chimera with M4, $5.8 \pm 1.2 \mu\text{M}$. Hence, a possible reason for the introduction of the M4 during the evolution could be the modification of the glutamate sensitivity.

In conclusion I showed that the pore exchange of a mammalian GluR by a potassium channel is possible. The main properties of both systems were still existing in the chimera. But there were some important points like the linker length and the choice of the used potassium channel to construct a functional glutamate gated potassium channel. This work could be offering a new experimental system to investigate structure/function correlations in complex glutamate receptors. In this kind of learning-by-building approach, channels could be engineered and combined to synthetic channels with defined properties to understand the interconnection of ligand sensing and pore opening.

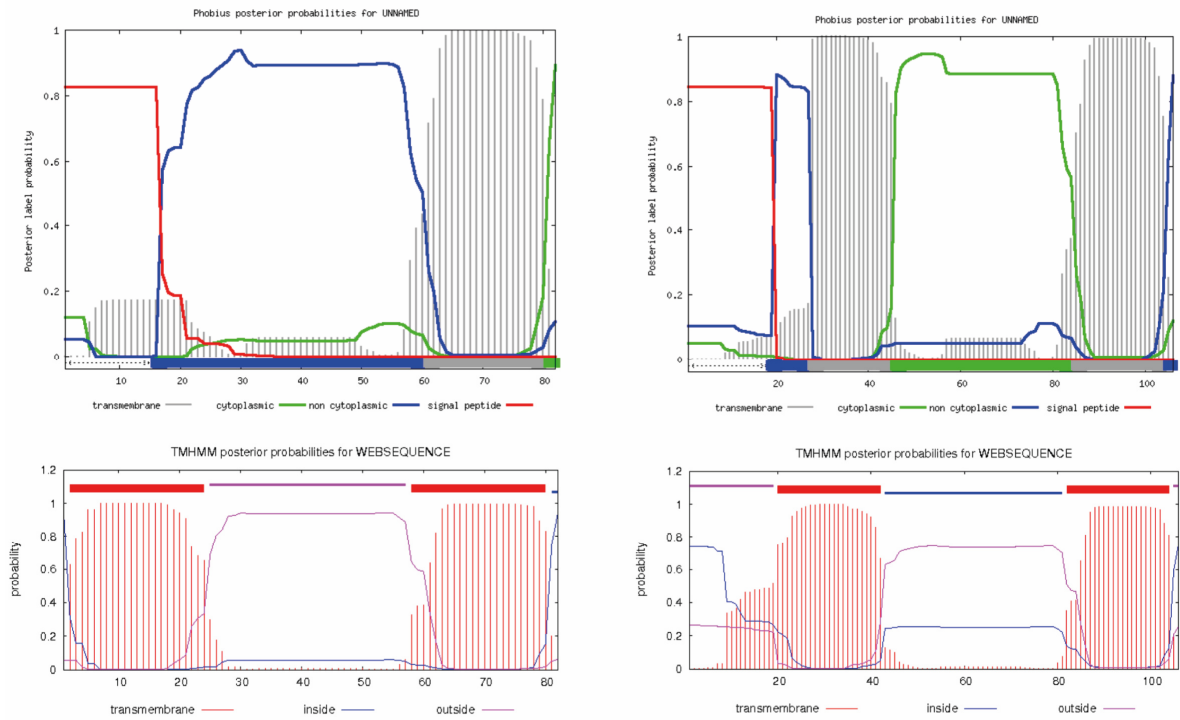
7. Supplement

Supplement 1 Table with the used Primer:

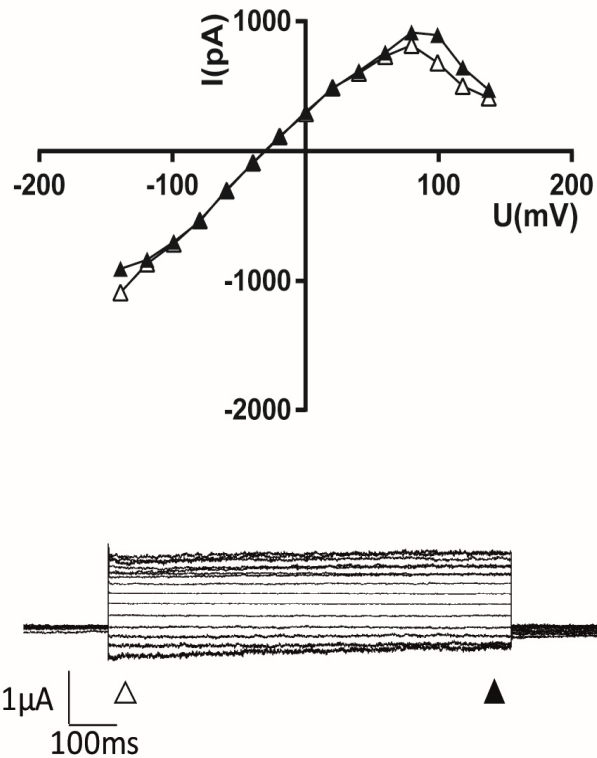
Primer name	Sequence 5` - 3`
Kcv _{ATCV-1} lin. fw	ATGTTGCTGCTTATCATAC
Kcv _{ATCV-1} lin. rw	AGCTTGCGGATCTG
HLA Insert I	ATGGCGGTGATGGCGCCGCGCACCCCTGGTGCTGCTGCTGAG CGGCGCGCTGGCGCTGACCCAGACCTGGGCGGGATTGCTG CTTATCATACA
HLA Insert II	CGCCCAGGTCTGGGTCAGCGCCAGCGCGCCGCTCAGCAGC AGCACCAGGGTGC GCGGCCATCACCGCCATAAGCTTGCG GATCTGACGG
TGN38 I	ATGCAGTTTCTGGTTGCCTTGCTTCTGCTTAGTGTGGCAG TCGCTCGGGCTATGTTGCTGCTTATCATACAT
TGN38 II	CATAGCCCGAGCGACTGCCACACTAAGCAGAAGCAAGGCA ACCAGAACTGCATAGCTTGCGGATCTGACG
β Insert I	ATGGGGCCACCCGGGAACGACAGTGACTTCTTGCTGACAA CCAACGGAAGCCATGTGCCAGACCACGATGTCACTGAGGA ACGGGACGAAGCATGGGTGGTAATGTTGCTGCTTATCATAC
β Insert II	TACCACCCATGCTTCGTCCCGTTCCTCAGTGACATCGTGG TCTGGCACATGGCTTCCGTTGGTTGTCAGCAAGAAGTCACT GTCGTTCCCGGGTGGCCCCATAGCTTGCGGATCTGACG
Kcv _{ATCV-1} Golgi M1G fw.	GCTCGGGCTGGGTTGCTGCT
Kcv _{ATCV-1} Golgi M1G rw.	AGCAGCAACCCAGCCCGAGC
Kcv _{ATCV-1} β M1G fw.	CATGGGTGGTAGGGTTGCTGC
Kcv _{ATCV-1} β M1G rw.	GCAGCAACCCTACCACCCATG
Kcv _{ATCV-1} HLA M1G fw.	CCTGGGCGGGGTTGCTGC
Kcv _{ATCV-1} HLA M1G rw.	GCAGCAACCCCGCCAGG
Myc-Tag fw.	AGCGAAGAGGACCTGTAAAGCGGCCGCG
Myc-Tag rw.	AATAAGCTTTTGTTCCTTGACAGCTCGTCCAT

Kcv_{ATCV-1}

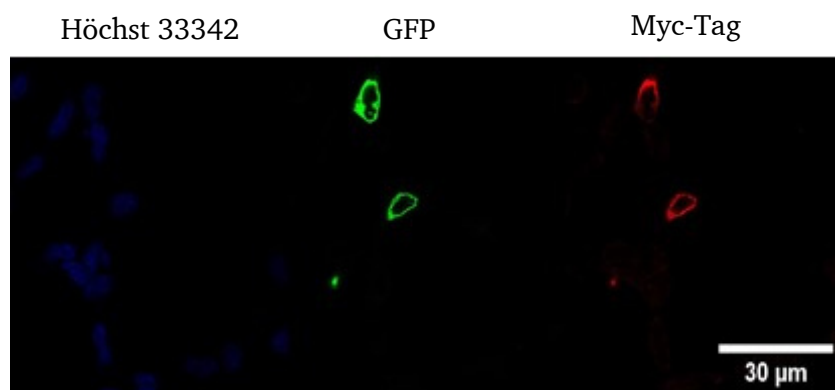
HLA-Kcv_{ATCV-1}



Supplement 2 Prediction of the orientation of Kcv_{ATCV-1} with and without the HLA signal peptide. On the left side you can see the prediction of Kcv_{ATCV-1}. The upper panel shows the prediction of Phobius in blue non-cytoplasmic regions and in green cytoplasmic ones. The pore building region between 24 and 60 AA is orientated to the cell outside. Down you can see the prediction of TMHMM regions outside the cell are colored in purple. The region between 25 and 60 is again located outside the cell. Using the signal peptide of HLA the prediction of Phobius shows an inverted picture. The pore region AA 25 to 60 is marked as inside the cell. In the second prediction tool the orientation is not clearly inverted.



Supplement 3 Representative patch clamp recording of an HEK cell expressing trans golgi network specific integral membrane protein TGN38 of rat coupled to Kcv_{ATCV-1} . The voltage current curve shows a linear influx and in more positive voltages a flattened outflux comparable to the HLA coupled one.



Supplement 4 Single image out of the CLSM stack of HLA-signal peptide coupled to the Kcv_{ATCV-1} with signals in the Myc-Tag (red) channel and with strong signals in the eGFP-channel (green). The fluorescent signal is located at the cell membrane for eGFP and also for the antibody staining against the Myc-tag. The nuclei are stained with Höchst33342 (blue). Scalebar: 30 μ M

8. Illustration directory

Figure 1 Topology of main potassium channel classes.....	6
Figure 2 Selectivity filter in potassium channels.	7
Figure 3 Structure of the AMPA GluA2.....	10
Figure 4 Conformational changes while the activation and inactivation of AMPA receptors.	12
Figure 5 Structure of Kcv _{ATCV-1} (red), KcsA (blue) and GluA2 (brown).	14
Figure 6 Patch clamp recording of an untransfected HEK293 cell.....	24
Figure 7 Representative patch clamp recording of a HEK cell expressing Kcv _{ATCV-1}	25
Figure 8 Representative patch clamp recording of an HEK cell expressing the HLA signal peptide coupled to Kcv _{ATCV-1} (HLA-Kcv _{ATCV-1}).....	26
Figure 9 Representative patch clamp recording of an HEK cell expressing the β -adrenergic signal peptide coupled to Kcv _{ATCV-1} (β -Kcv _{ATCV-1}).....	27
Figure 10 Overview of the 3 Kcv _{ATCV-1} constructs.	28
Figure 11 Rectification coefficient for the Kcv _{ATCV-1} and signal peptide coupled Kcv _{ATCV-1}	29
Figure 12 Strategy for detecting the direction of the Kcv _{ATCV-1}	30
Figure 13 Maximum intensity projection of CLSM image of Kcv _{ATCV-1} coupled to eGFP ..	31
Figure 14 Maximum intensity projection of CLSM image of HLA-Kcv _{ATCV-1}	31
Figure 15 Maximum intensity projection of CLSM image of β - Kcv _{ATCV-1}	32
Figure 16 Fluorescence integrated density of Myc-Tag in relation to GFP signal.....	32
Figure 17 Design of Kcv _{ATCV-1} /GluA1chimeras.	40
Figure 18 Functional characterization of chimeric GluATCV constructs.....	41
Figure 19: Influence of the open probability of Kcv _{ATCV-1} by TM2 point mutations.....	43
Figure 20 Increase of Glu-gating efficiency in GluATCV by TM2 point mutations.....	44
Figure 21 Functional characterization of the GluATCV chimera..	45
Figure 22 Potassium selectivity of GluATCV*.....	46
Figure 23 Schematic drawings and functional expression of the deletion and mutant constructs used.....	52
Figure 24 Functionality of the used mutants.....	53

9. List of abbreviations

-°C	degree Celsius
-μL	micro liter
-AA	amino acids
-AMPA	2-Amino-3-(3-hydroxy-5-methyl-isoxazol-4-yl)propanoic acid
-Ba ⁺	barium
-BSA	bovine serum albumin
-CaCl ₂	calcium dichloride
-CLSM	confocal laser scanning microscope
-CO ₂	carbon dioxide
-dATP	deoxyadenosine triphosphate
-dCTP	deoxycytidine triphosphate
-dGTP	deoxygenizing triphosphate
-DNA	deoxyribonucleic acid
-dTTP	deoxythymidine triphosphate
-EGTA	Ethylene glycol-bis(2-aminoethylether)-N,N,N',N'-tetraacetic acid
-β	β adrenergic receptor
-FCS	fetal calf serum
-GFP	green fluorescent protein
-GFP/eGFP	green fluorescent protein/ enhanced green fluorescent protein
-glu	glutamate
-HEK293	human embryonic kidney cell 293
-HEPES	2-[4-(2-hydroxyethyl)piperazin-1-yl]ethanesulfonic acid
-HLA	human-leucocyte-antigen class1
-I	current
-I _{Ba}	barium blockable current
-I _{Glu}	glutamate induced current
-I _{leak}	leakage current
-K ⁺	potassium
-kcal	kilo calorie
-KCl	potassium chloride
-Kcv	potassium channel out of chlorella virus
-KOH	Potassium hydroxide
-MEM	minimum essential media
-MgCl ₂	Magnesium dichloride

-min	minute
-ml	milliliter
-mM	milli molar
-ms	milli second
-mV	milli voltage
-Na ⁺	sodium
-NaCl	sodium chloride
-ng	nano gram
-NMDA	(2R)-2-(Methylamino)butanedioic acid
-NTD	n-terminal domain
-pA	pico Ampere
-PBG	phosphate buffered saline with gelatin
-PBS	phosphate buffered saline
-PDB	protein data bank
-Pen/Strep	penicillin/streptomycin
-PFA	paraformaldehyde
-PNK	poly nucleotide kinase
-Po	open probability
-pS	pico siemens
-rpm	rounds per minute
-s	second
-SEM	standard error of the mean
-T25	flask with 25 cm ²
-TM/TMD	transmembrane domain
-TGN38	trans golgi network specific integral membrane protein TGN38 of rat
-V	voltage
-Ω	Ohm

10. References

- Amin, J.B. et al., 2017. Divergent roles of a peripheral transmembrane segment in AMPA and NMDA receptors. *Journal of General Physiology*, 149(6), pp.1–20.
- Anderson, P. a & Greenberg, R.M., 2001. Phylogeny of ion channels: clues to structure and function. *Comparative Biochemistry and Physiology Part B*, 129(1), pp.17–28. Available at: <http://www.ncbi.nlm.nih.gov/pubmed/11337248>.
- Arinaminpathy, Y. et al., 2003. A prokaryotic glutamate receptor: Homology modelling and molecular dynamics simulations of GluR0. *FEBS Letters*, 553(3), pp.321–327.
- Armstrong, C.M. & Taylor, S.R., 1980. Interaction of barium ions with potassium channels in squid giant axons. *Biophysical Journal*, 30(3), pp.473–488. Available at: [http://dx.doi.org/10.1016/S0006-3495\(80\)85108-3](http://dx.doi.org/10.1016/S0006-3495(80)85108-3).
- Armstrong, N. & Gouaux, E., 2000. Mechanisms for Activation and Antagonism of an AMPA-Sensitive Glutamate Receptor : Crystal Structures of the GluR2 Ligand Binding Core. , 28, pp.165–181.
- Arrigoni, C. et al., 2013. The voltage-sensing domain of a phosphatase gates the pore of a potassium channel. *The Journal of General Physiology*, 141(3), pp.389–395. Available at: <http://www.jgp.org/lookup/doi/10.1085/jgp.201210940>.
- Ayalon, G. et al., 2001. Functional assembly of AMPA and kainate receptors is mediated by several discrete protein-protein interactions. *Neuron*, 31(1), pp.103–113. Available at: <http://www.ncbi.nlm.nih.gov/pubmed/11498054>.
- Bavro, V.N. et al., 2012. Structure of a KirBac potassium channel with an open bundle crossing indicates a mechanism of channel gating. *Nature Structural and Molecular Biology*, 19(2), pp.158–164.
- Berneche, S. & Roux, B., 2001. Energetics of ion conduction through the K⁺ channel. *Nature*, 414(November). Available at: <http://www.nature.com/nature/journal/v414/n6859/abs/414073a0.html> [Accessed April 27, 2014].
- Berntsson, R.P.-A. et al., 2010. A structural classification of substrate-binding proteins. *FEBS letters*, 584(12), pp.2606–2617. Available at: <http://dx.doi.org/10.1016/j.febslet.2010.04.043>.
- Chang, H.-R. & Kuo, C.-C., 2008. The Activation Gate and Gating Mechanism of the NMDA Receptor. *Journal of Neuroscience*, 28(7), pp.1546–1556. Available at: <http://www.jneurosci.org/cgi/doi/10.1523/JNEUROSCI.3485-07.2008>.
- Chatelain, F.C. et al., 2005. The pore helix dipole has a minor role in inward rectifier channel

-
- function. *Neuron*, 47(6), pp.833–843. Available at: <http://www.sciencedirect.com/science/article/pii/S0896627305006975> [Accessed May 20, 2014].
- Chen, G.-Q. et al., 1999. Functional characterization of a potassium-selective prokaryotic glutamate receptor. *Nature*, 402(6763), pp.817–821.
- Chiu, J. et al., 1999. Molecular evolution of glutamate receptors: a primitive signaling mechanism that existed before plants and animals diverged. *Molecular biology and evolution*, 16(6), pp.826–838.
- Cosentino, C. et al., 2015. Engineering of a light-gated potassium channel. *Science*, 348(6235), pp.707–710. Available at: <http://www.sciencemag.org/cgi/doi/10.1126/science.aaa2787>.
- Dai, J., Wollmuth, L.P. & Zhou, H.X., 2015. Mechanism-Based Mathematical Model for Gating of Ionotropic Glutamate Receptors. *Journal of Physical Chemistry B*, 119(34), pp.10934–10940.
- DiFrancesco, M.L. et al., 2015. Engineering a Ca⁺⁺-sensitive (Bio)sensor from the pore-module of a potassium channel. *Sensors (Switzerland)*, 15(3), pp.4913–4924.
- Dingledine, R. et al., 1999. The glutamate receptor ion channels. *Pharmacol.Rev.*, 51(1), pp.7–61. Available at: <http://www.ncbi.nlm.nih.gov/pubmed/15218076>.
- Doyle, D. a. et al., 1998. The Structure of the Potassium Channel: Molecular Basis of K⁺ Conduction and Selectivity. *Science*, 280(5360), pp.69–77. Available at: <http://www.sciencemag.org/cgi/doi/10.1126/science.280.5360.69> [Accessed March 19, 2014].
- Doyle, D.A., 2004. Structural changes during ion channel gating. *Trends in Neurosciences*, 27(6), pp.298–302.
- Egebjerg, J. & Heinemann, S.F., 1993. Ca²⁺ permeability of unedited and edited versions of the kainate selective glutamate receptor GluR6. *Proceedings of the National Academy of Sciences of the United States of America*, 90(2), pp.755–9. Available at: <http://www.pubmedcentral.nih.gov/articlerender.fcgi?artid=45744&tool=pmcentrez&rendertype=abstract>.
- Ferrer-Montiel, A. V., Sun, W. & Montal, M., 1996. A single tryptophan on M2 of glutamate receptor channels confers high permeability to divalent cations. *Biophysical Journal*, 71(2), pp.749–758. Available at: [http://dx.doi.org/10.1016/S0006-3495\(96\)79274-3](http://dx.doi.org/10.1016/S0006-3495(96)79274-3).
- Di Francesco, M., 2011. *Analysis of inherent properties of Ion Channels from PBCV-1 Chlorella virus and Influenza A virus*. Dissertation Universität Mailand.
- Furukawa, H., 2012. Structure and function of glutamate receptor amino terminal domains.

-
- Journal of Physiology*, 590(1), pp.63–72.
- Gan, Q., Salussolia, C.L. & Wollmuth, L.P., 2015. Assembly of AMPA receptors: mechanisms and regulation. *The Journal of Physiology*, 593(1), pp.39–48. Available at: <http://www.pubmedcentral.nih.gov/articlerender.fcgi?artid=4293052&tool=pmcentrez&rendertype=abstract>.
- Gazzarrini, S. et al., 2009. Chlorella virus ATCV-1 encodes a functional potassium channel of 82 amino acids. *Biochem. J*, 420(2), pp.295–303. Available at: <http://biochemj.org/lookup/doi/10.1042/BJ20090095> [Accessed November 11, 2013].
- Gazzarrini, S. et al., 2003. The viral potassium channel Kcv: Structural and functional features. *FEBS Letters*, 552(1), pp.12–16.
- Hartmann, E., Rapoport, T.O.M.A. & Lodisht, H.F., 1989. Predicting the orientation of eukaryotic membranespanning proteins. , 86(August), pp.5786–5790. Available at: <papers2://publication/uuid/22F936F7-2FFF-4D47-B08B-10933035337A>.
- Heginbotham, L. et al., 1994. Mutations in the K⁺ channel signature sequence. *Biophys. J.*, 66(4), pp.1061–7. Available at: <http://www.pubmedcentral.nih.gov/articlerender.fcgi?artid=2606936&tool=pmcentrez&rendertype=abstract>.
- Hibino, H. et al., 2010. Inwardly Rectifying Potassium Channels: Their Structure, Function, and Physiological Roles. *Physiological Reviews*, 25(2), pp.291–366.
- Hille, B., 2001. Ion Channel Excitable Membranes. *Sunderland Massachusetts USA*, pp.1–37.
- Hodgkin, A.L. & Huxley, A.F., 1952. A quantitative description of membrane current and its application to conduction and excitation in nerve. *The Journal of physiology*, 117(4), pp.500–544. Available at: <https://www.ncbi.nlm.nih.gov/pubmed/12991237>.
- Hoffmann, J. et al., 2006. Investigation via ion pore transplantation of the putative relationship between glutamate receptors and K⁺ channels. *Molecular and cellular neurosciences*, 33(4), pp.358–70. Available at: <http://www.ncbi.nlm.nih.gov/pubmed/17011207> [Accessed October 7, 2014].
- Iglesias, A. et al., 2017. Serotonin 2A receptor disulfide bridge integrity is crucial for ligand binding to different signalling states but not for its homodimerization. *European Journal of Pharmacology*, 815(August), pp.138–146. Available at: <http://dx.doi.org/10.1016/j.ejphar.2017.09.011>.
- Janovjak, H., Sandoz, G. & Isacoff, E.Y., 2011. A modern ionotropic glutamate receptor with a K⁺ selectivity signature sequence. *Nature Communications*, 2, p.232. Available at: <http://www.nature.com/doi/10.1038/ncomms1231>.
- Jiang, Y. et al., 2002. Crystal structure and mechanism of a calcium-gated potassium channel.

-
- , pp.515–522.
- Kalckar, H.M., 1971. The periplasmic galactose binding protein of *Escherichia coli*. *Science*, 174(4009), pp.557–565.
- Kandel, E.R., Schwartz, J.H. & Jessell, T.M., 1995. *Essentials of Neural Science and Behavior*, McGraw-Hill. Available at: <https://books.google.de/books?id=1kFqAAAAMAAJ>.
- Karakas, E. & Furukawa, H., 2014. Crystal structure of a heterotetrameric NMDA receptor ion channel. *Science*, 344(6187), pp.992–997. Available at: <http://www.sciencemag.org/cgi/doi/10.1126/science.1251915> [Accessed May 29, 2014].
- Kazi, R. et al., 2014. Mechanical coupling maintains the fidelity of NMDA receptor-mediated currents. *Nature Neuroscience*, 17(7), pp.914–922.
- Kott, S. et al., 2009. Comparative analysis of the pharmacology of GluR1 in complex with transmembrane AMPA receptor regulatory proteins $\gamma 2$, $\gamma 3$, $\gamma 4$, and $\gamma 8$. *Neuroscience*, 158(1), pp.78–88. Available at: <http://dx.doi.org/10.1016/j.neuroscience.2007.12.047>.
- Krieger, J., Bahar, I. & Greger, I.H., 2015. Structure, Dynamics, and Allosteric Potential of Ionotropic Glutamate Receptor N-Terminal Domains. *Biophysical Journal*, 109(6), pp.1136–1148. Available at: <http://dx.doi.org/10.1016/j.bpj.2015.06.061>.
- Krogh, A. et al., 2001. Predicting transmembrane protein topology with a hidden Markov model: Application to complete genomes. *Journal of Molecular Biology*, 305(3), pp.567–580.
- Krogh, A., Sonnhammer, E.L.L. & Ka, L., 2004. A Combined Transmembrane Topology and Signal Peptide Prediction Method. , pp.1027–1036.
- Kuang, Q., Purhonen, P. & Hebert, H., 2015. Structure of potassium channels. *Cellular and Molecular Life Sciences*, 72(19), pp.3677–3693.
- Kumar, J. & Mayer, M.L., 2013. Functional insights from glutamate receptor ion channel structures. *Annual review of physiology*, 75, pp.313–37. Available at: <http://www.pubmedcentral.nih.gov/articlerender.fcgi?artid=4130219&tool=pmcentrez&rendertype=abstract> [Accessed September 4, 2014].
- Kuner, T., Seeburg, P.H. & Guy, H.R., 2003. A common architecture for K⁺ channels and ionotropic glutamate receptors? *Trends in Neurosciences*, 26(1), pp.27–32.
- Kuo, M.M.C. et al., 2005. Prokaryotic K⁺ channels: From crystal structures to diversity. *FEMS Microbiology Reviews*, 29(5), pp.961–985.
- Lüttge, G., Kluge, M. & Thiel, G., 2010. *Botanik - Die umfassende Biologie der Pflanzen*,
- Lynagh, T., Kunz, A. & Laube, B., 2013. Propofol modulation of $\alpha 1$ glycine receptors does not require a structural transition at adjacent subunits that is crucial to agonist-induced

-
- activation. *ACS Chemical Neuroscience*, 4(11), pp.1469–1478.
- Lynagh, T. & Laube, B., 2014. Opposing Effects of the Anesthetic Propofol at Pentameric Ligand-Gated Ion Channels Mediated by a Common Site. *Journal of Neuroscience*, 34(6), pp.2155–2159. Available at: <http://www.jneurosci.org/cgi/doi/10.1523/JNEUROSCI.4307-13.2014>.
- MacKinnon, R., 2004. Potassium Channels and the Atomic Basis of Selective Ion Conduction (Nobel Lecture). *Angewandte Chemie International Edition*, 43(33), pp.4265–4277. Available at: <https://onlinelibrary.wiley.com/doi/abs/10.1002/anie.200400662>.
- Madry, C. et al., 2007. The N-Terminal Domains of both NR1 and NR2 Subunits Determine Allosteric Zn²⁺ Inhibition and Glycine Affinity of N-Methyl-D-aspartate Receptors. *Molecular Pharmacology*, 72(6), pp.1535–1544. Available at: <http://molpharm.aspetjournals.org/cgi/doi/10.1124/mol.107.040071>.
- Mayer, M.L., Olson, R. & Gouaux, E., 2001. Mechanisms for ligand binding to GluR0 ion channels: crystal structures of the glutamate and serine complexes and a closed apo state. *Journal of molecular biology*, 311(4), pp.815–836.
- Mesic, I. et al., 2016. The N-terminal domain of the GluN3A subunit determines the efficacy of glycine-activated NMDA receptors. *Neuropharmacology*, 105, pp.133–141. Available at: <http://dx.doi.org/10.1016/j.neuropharm.2016.01.014>.
- Miller, C., 2000. An overview of the potassium channel family. *Genome biology*, 1(4), p.REVIEWS0004. Available at: <http://www.pubmedcentral.nih.gov/articlerender.fcgi?artid=138870&tool=pmcentrez&rendertype=abstract>.
- Montal, M. & Mueller, P., 1972. Formation of Bimolecular Membranes from Lipid Monolayers and a Study of Their Electrical Properties. *Proceedings of the National Academy of Sciences*, 69(12), pp.3561–3566. Available at: <http://www.pnas.org/cgi/doi/10.1073/pnas.69.12.3561>.
- Moore, B.S. et al., 2013. A conserved mechanism for gating in an ionotropic glutamate receptor. *Journal of Biological Chemistry*, 288(26), pp.18842–18852.
- Mowbray, S.L. & Petsko, G.A., 1983. The x-ray structure of the periplasmic galactose binding protein from *Salmonella typhimurium* at 3.0-Å resolution. *Journal of Biological Chemistry*, 258(13), pp.7991–7997.
- O'Hara, P.J. et al., 1993. The ligand-binding domain in metabotropic glutamate receptors is related to bacterial periplasmic binding proteins. *Neuron*, 11, pp.41–52.
- Ooi, A. et al., 2016. A guide to transient expression of membrane proteins in HEK-293 cells for functional characterization. *Frontiers in Physiology*, 7(JUL), pp.1–15.

-
- Parsegian, A., 1969. Energy of an ion crossing a low dielectric membrane: solutions to four relevant electrostatic problems. *Nature*. Available at: [http://alevine.chem.ucla.edu/187/Parsegian VA Energy of an ion crossing Nature 221 pp844-6 1969.pdf](http://alevine.chem.ucla.edu/187/Parsegian%20VA%20Energy%20of%20an%20ion%20crossing%20Nature%20221%20pp844-6%201969.pdf) [Accessed February 5, 2014].
- Pasternack, A. et al., 2002. α -amino-3-hydroxy-5-methyl-4-isoxazolepropionic acid (AMPA) receptor channels lacking the N-terminal domain. *Journal of Biological Chemistry*, 277(51), pp.49662–49667.
- Patten, C.D. et al., 1999. Structural and functional modularity of voltage-gated potassium channels. , 463, pp.375–381.
- Pettersen, E.F. et al., 2004. UCSF Chimera - A visualization system for exploratory research and analysis. *Journal of Computational Chemistry*, 25(13), pp.1605–1612.
- Piasta, K.N., Theobald, D.L. & Miller, C., 2011. Potassium-selective block of barium permeation through single KcsA channels. *The Journal of General Physiology*, 138(4), pp.421–436. Available at: <http://www.jgp.org/lookup/doi/10.1085/jgp.201110684>.
- Price, M.B., Jelesko, J. & Okumoto, S., 2012. Glutamate Receptor Homologs in Plants: Functions and Evolutionary Origins. *Frontiers in Plant Science*, 3(October), pp.1–10. Available at: <http://journal.frontiersin.org/article/10.3389/fpls.2012.00235/abstract>.
- Quiocho, F.A. & Pflugrath, J.W., 1980. The structure of D-galactose-binding protein at 4.1 Å resolution looks like L-arabinose-binding protein. *Journal of Biological Chemistry*, 255(14), pp.6559–6551.
- Rauh, O. et al., 2017. Identification of Intrahelical Bifurcated H-Bonds as a New Type of Gate in K⁺ Channels. *Journal of the American Chemical Society*, 139(22), pp.7494–7503.
- Rowley, C.N. & Roux, B., 2013. A computational study of barium blockades in the KcsA potassium channel based on multi-ion potential of mean force calculations and free energy perturbation. *The Journal of General Physiology*, 142(4), pp.451–463. Available at: <http://www.jgp.org/lookup/doi/10.1085/jgp.201311049>.
- Saglietti, L. et al., 2007. Extracellular Interactions between GluR2 and N-Cadherin in Spine Regulation. *Neuron*, pp.461–477.
- Salussolia, C.L. et al., 2013. A Eukaryotic Specific Transmembrane Segment is Required for Tetramerization in AMPA Receptors. *Journal of Neuroscience*, 33(23), pp.9840–9845. Available at: <http://www.jneurosci.org/cgi/doi/10.1523/JNEUROSCI.2626-12.2013>.
- Salussolia, C.L. et al., 2011. Interaction of the M4 segment with other transmembrane segments is required for surface expression of mammalian α -amino-3-hydroxy-5-methyl-4-isoxazolepropionic acid (AMPA) receptors. *Journal of Biological Chemistry*, 286(46), pp.40205–40218. Available at:

- <http://www.pubmedcentral.nih.gov/articlerender.fcgi?artid=3220572&tool=pmcentrez&rendertype=abstract> [Accessed October 7, 2014].
- Schmid, S.M. et al., 2007. A domain linking the AMPA receptor agonist binding site to the ion pore controls gating and causes lurcher properties when mutated. *The Journal of neuroscience: the official journal of the Society for Neuroscience*, 27(45), pp.12230–41. Available at: <http://www.ncbi.nlm.nih.gov/pubmed/17989289> [Accessed October 7, 2014].
- Schorge, S. & Colquhoun, D., 2003. Studies of NMDA Receptor Function and Stoichiometry with Truncated and Tandem Subunits. *J. Neurosci.*, 23(4), pp.1151–1158. Available at: <http://www.jneurosci.org/content/23/4/1151.long>.
- Schönrock, M., Thiel, G. & Laube, B., 2019. Coupling of a viral K⁺-channel with a glutamate-binding-domain highlights the modular design of ionotropic glutamate-receptors. *Communications Biology*, (2019), pp.1–10. Available at: <http://dx.doi.org/10.1038/s42003-019-0320-y>.
- Sobolevsky, A.I., 2015. Structure and gating of tetrameric glutamate receptors. *Journal of Physiology*, 593(1), pp.29–38.
- Sobolevsky, A.I., Rosconi, M.P. & Gouaux, E., 2009. X-ray structure, symmetry and mechanism of an AMPA-subtype glutamate receptor. *Nature*, 462(7274), pp.745–56. Available at: <http://www.nature.com/nature/journal/v462/n7274/full/nature08624.html#B1> [Accessed July 14, 2014].
- Sobolevsky, A.I., Rosconi, M.P. & Gouaux, E., 2010. X-ray structure of AMPA-subtype glutamate receptor: symmetry and mechanism. *Nature*, 462(7274), pp.745–756.
- Sobolevsky, A.I., Yelshansky, M. V & Wollmuth, L.P., 2003. Different Gating Mechanisms in Glutamate Receptor and K⁺ Channels. *The Journal of neuroscience*, 23(20), pp.7559–7568.
- Stern-Bach, Y. et al., 1998. A point mutation in the glutamate binding site blocks desensitization of AMPA receptors. *Neuron*, 21, pp.907–918. Available at: <http://www.sciencedirect.com/science/article/pii/S0896627300806054> [Accessed October 7, 2014].
- Tayefeh, S. et al., 2009. Model development for the viral Kcv potassium channel. *Biophysical Journal*, 96(2), pp.485–498. Available at: <http://dx.doi.org/10.1016/j.bpj.2008.09.050>.
- Thiel, G. et al., 2011. Minimal art: or why small viral K(+) channels are good tools for understanding basic structure and function relations. *Biochim. Biophys. acta*, 1808(2), pp.580–8. Available at: <http://www.ncbi.nlm.nih.gov/pubmed/20417613> [Accessed April 21, 2014].
- Thiel, G. et al., 2013. Potassium ion channels: could they have evolved from viruses? *Plant*

-
- physiology*, 162(3), pp.1215–24. Available at: <http://www.ncbi.nlm.nih.gov/pubmed/23719891> [Accessed March 24, 2014].
- Tikhonov, D.B. & Magazanik, L.G., 2009. Origin and molecular evolution of ionotropic glutamate receptors. *Neuroscience and Behavioral Physiology*, 39(8), pp.763–773.
- Traynelis, S.F. et al., 2010. Glutamate Receptor Ion Channels: Structure, Regulation, and Function. *Pharmacological Reviews*, 14(1), pp.37–40.
- Traynelis, S.F., Lonnie P. Wollmuth, Chris J. McBain, Frank S. Menniti, Katie M. Vance, Kevin K. Ogden, Kasper B. Hansen, Hongjie Yuan, S.J.M. & Dingledine, R., 2010. Glutamate Receptor Ion Channels: Structure, Regulation, and Function Stephen. *Catheterization and cardiovascular diagnosis*, 14(1), pp.37–40.
- Twomey, E.C. et al., 2017. Channel opening and gating mechanism in AMPA-subtype glutamate receptors. *Nature*, 549(7670), pp.60–65. Available at: <http://dx.doi.org/10.1038/nature23479>.
- Uysal, S. et al., 2009. Crystal structure of full-length KcsA in its closed conformation. *Proceedings of the National Academy of Sciences*, 106(16), pp.6644–6649. Available at: <http://www.pnas.org/cgi/doi/10.1073/pnas.0810663106>.
- Waschutzka, G. et al., 1996. Engineered disulfide bonds in recombinant human interferon-gamma: the impact of the N-terminal helix A and the AB-loop on protein stability. *Protein Engineering*, 9(10), pp.905–912.
- White, S.L. et al., 2016. A Critical Role for the GluA1 Accessory Protein, SAP97, in Cocaine Seeking. *Neuropsychopharmacology*, 41(3), pp.736–750. Available at: <http://dx.doi.org/10.1038/npp.2015.199>.
- Wilcox, T. & Hirshkowitz, A., 2015. Deletion of the N-terminal Domain (NTD) Alters the Ethanol Inhibition of NMDA Receptors in a Subunit-Dependent Manner. , 85(0 1), pp.1–27.
- Winterstein, L.-M. et al., 2018. Reconstitution and functional characterization of ion channels from nanodiscs in lipid bilayers. *The Journal of General Physiology*, 150(4), p.637 LP-646. Available at: <http://jgp.rupress.org/content/150/4/637.abstract>.
- Wollmuth, L.P. & Sobolevsky, A.I., 2004. Structure and gating of the glutamate receptor ion channel. *Trends in Neurosciences*, 27(6), pp.321–328.
- Wood, M.W., VanDongen, H.M. & VanDongen, A.M., 1995. Structural conservation of ion conduction pathways in K channels and glutamate receptors. *Proceedings of the National Academy of Sciences of the United States of America*, 92(11), pp.4882–6. Available at: <http://www.pubmedcentral.nih.gov/articlerender.fcgi?artid=41811&tool=pmcentrez&rendertype=abstract>.

11. Curriculum Vitae

Name: Michael Schönrock
Date of birth: December 23 th, 1988
Place of birth: Heidelberg
Nationality: German

Education:

2014-2018:

Doctoral candidate at TU Darmstadt in the group of Prof. Dr. Bodo Laube, department of Neurophysiology and Neurosensory Systems.

2012-2014

Master of Sciences “Technische Biologie” at TU Darmstadt

Master thesis: “Konstruktion und Charakterisierung von Chimären aus verschiedenen viralen Kaliumkanälen: Die funktionale Bedeutung der Turret-domäne” in the group of Prof. Dr. Gerhard Thiel, department of Plant Membrane Biophysics.

2009-2012

Bachelor of Science “Biologie” at Tu Darmstadt

Bachelor thesis: “Einzelkanalstudien zum Cs⁺-Block am viralen K⁺-Kanal Kcv_{ATCV-1}” in the group of Prof. Dr. Gerhard Thiel, department of Plant Membrane Biophysics.

2008

Abitur at Dietrich-Bonhoeffer-Gymnasium, Eppelheim

Poster, Talks and Publikation:

Paper published in communications biology (2019)

“Coupling of a viral K⁺-channel with a glutamate-binding-domain highlights the modular design of ionotropic glutamate-receptors.” (Michael Schönrock, Gerhard Thiel, Bodo Laube)

Student Talk and poster presentation at 61st annual meeting of the Biophysical Society

“Design of a glutamate-activated potassium channel upon fusion of the ligand-binding domain of the mammalian AMPA-receptor GluA1 to the channel pore of the viral Kcv_{ATCV-1} K⁺ channel”

12. Acknowledgement

I would like to thank ...

... first of all Prof. Dr. Bodo Laube for giving me the opportunity to work on this interesting project, for the freedom in trying different ways of solution, for the helpful discussions and that I could always ask when I was faced with seemingly insoluble problems.

... Prof. Dr. Gerhard Thiel for being the co-referee of this thesis and that he also always had an open ear for me. Also, a great thank to my other examiners Prof. Dr. Süß and Prof. Dr. Ensinger.

... Dr. Indra Schroeder for the helpful discussions about the orientation of potassium channel.

... my room partners Axel, Kai, Gabi and the lost one Vito for much fun between the analysis time and the important and much more for the non-important discussions.

... the kicker group Oli, Axel, Katja, Kerri, Patrick, Sebastian,

... to the complete AG Laube! Selina, Henrik, Max, Basti, Kiki, Katja, Hannah, Raj, Michel, Alex, Axel, Kai, Gabi, Chris, Kirsten, Juliane and everyone I forgotten to mention and also to the AG Thiel.

Finally, I want to thank my whole family for the support in the last years; at my mum, my dad and my sister and not to forget my grandma. Thanks to Chrissi for the last seven years and all the upcoming.

